



MSc INDIVIDUAL REPORT

Experimental and Numerical Modelling of Coastal Processes

Author:
Jacob VAN ALWON

Supervisors:
Prof. Onno BOKHOVE
Dr. Duncan BORMAN

ABSTRACT:

Wave overtopping can cause flooding in coastal regions, posing risks to individuals and property. The design of coastal defences is therefore of high importance so that the volume of water overtopped is minimised. JBA group require a wave tank to be designed which clearly demonstrates how various coastal defence configurations affect overtopping under a range of wave conditions. The design of this tank is informed by experiments conducted in a test tank. The experiments show a range of overtopping rates for different coastal defences. The test tank is modelled using the open source Smoothed Particle Hydrodynamics (SPH) software, DualSPHysics. The SPH simulations accurately predict the free surface profiles for a range of wave conditions and coastal defences, however overtopping is considerably underestimated.

MECH5870M Team Project:
Wave Tank Design and Build

Student: Jacob van Alwon
Supervisors: Prof. Onno Bokhove
Dr. Duncan Borman
19/06/2015

Contents

1	Introduction	1
2	Coastal Flood Risk	1
2.1	Performance of Coastal Defences	2
2.2	Industry Practice	3
3	Similitude	3
3.1	Scaling	4
4	Experimental Procedure	5
4.1	Data Analysis	8
4.2	Experimental Error	9
5	Smoothed Particle Hydrodynamics (SPH) Theory	10
5.1	Smoothing Kernel	11
5.2	Compressibility	11
5.3	Viscosity Treatment	12
5.4	δ -SPH	13
6	SPH Implementation Methodology	13
6.1	Initial Particle Independence Study	15
6.2	Sound Speed Sensitivity Analysis	15
6.3	Test Cases	16
6.3.1	Unforced Case	16
6.3.2	Forced Case	16
6.4	Revised Particle Independence Study	17
6.5	Conclusions of SPH Implementation Studies	18
7	Results	18
7.1	Repeatability	18
7.2	Experimental Wave Overtopping	18
7.3	Determination of δ -SPH	20
7.4	Continuous Waves	21
7.5	Single Wave	24
7.6	Standing Wave	25
7.7	Simulated Wave Overtopping	26
8	Insert and Tank Design	28
9	Conclusions	30

A SPH Implementation	33
A.1 Initial Particle Independence Study	34
A.2 Sound Speed Sensitivity Analysis	37
A.3 Test Cases	43
A.3.1 Unforced Case	43
A.3.2 Forced Case	45
A.4 Revised Particle Independence Study	48
A.5 Conclusions of SPH Implementation Studies	50
B Further Results	50
B.1 Single Wave	50
B.1.1 Vertical Wall	50
B.1.2 1 in 2 Slope	51
B.1.3 1 in 3 Slope	51
B.1.4 Stepped Slope	52
B.1.5 Recurved Wall	52
B.2 Continuous Wave	53
B.2.1 Vertical Wall	53
B.2.2 1 in 2 Slope	54
B.2.3 1 in 3 Slope	55
B.2.4 Stepped Slope	56
B.2.5 Recurved Wall	57

1 Introduction

The aim of this investigation is to design a wave tank for use by JBA Trust, a non-profit organisation which promotes scientific research, education and training in the fields of environmental risk and resources (JBA Consulting, 2015). JBA Trust is a subsidiary of JBA Consulting, an environmental engineering group which works in several environmental fields including flood risk and coastal management (JBA Consulting, 2015). The wave tank is to be used to demonstrate the overtopping rates of various coastal defences when subjected to a range of wave conditions. The dimensions of the tank are restricted to a 200mm × 183mm cross section and a 1600mm length so that it is easily transportable. The coastal defences must be designed to be easily inserted and removed so that many coastal processes can be demonstrated within a reasonable time frame.

Experiments are carried out in a test tank in order to inform the design of the demonstration tank. Simulations of the experiments are carried out using Smoothed Particle Hydrodynamics (SPH) and the overtopping rates and free surface profiles compared to the experimental data.

The author's primary responsibilities are the design of the coastal defences, SPH numerical modelling, data collection and analysis and scaling between true coastal processes and the laboratory model. The author has also partly focussed on the construction of the wave maker and the design of the wave tank.

Objectives

In order to achieve the project aim the following objectives are completed:

- The wave conditions in the tank are scaled to real life wave conditions around the British coast.
- Experiments are conducted in a test tank to inform the design of the final demonstration tank.
- Image analysis software is used to measure the free surface level in the experiments.
- Investigation into key SPH parameters is conducted to find appropriate values for simulation of the wave tank.
- The wave tank experiments are simulated in SPH and the results are compared to establish whether the modelling technique used can make reliable predictions about real flows.

2 Coastal Flood Risk

Management of coastal flood risk is an important issue as sea waves which bypass coastal defences, especially in storm conditions, can cause serious damage to properties and pose a safety risk to members of the public. Therefore it is important that coastal defences are designed to minimise the amount of water that is overtopped within an appropriate factor of safety.

2.1 Performance of Coastal Defences

The interaction between a wave and a coastal defence can be divided into three categories. These categories are described by (Thomas and Hall, 1992).

Reflection

A proportion of the wave energy impacting a sea wall will always be reflected seaward. A vertical, impermeable sea wall will reflect almost all of the energy of a wave providing that the wall is of sufficient height. Although this may be an efficient method of preventing overtopping it can have detrimental effects on conditions seaward of the wall. After a wave is reflected it will superpose with incident waves approaching the wall, creating a wave height that is the sum of the heights of the two waves. This superposition of waves increases wave action in front of the wall and can increase the potential for sediment transport as well as producing localised scour which can undermine the foundation of the wall.

Wave reflection is affected by the roughness, porosity and slope of a coastal defence. Defences with a high roughness or porosity will reflect less wave energy than smooth or non-porous walls and vertical walls will reflect more wave energy than sloped walls. Wave characteristics also affect reflection, for example, long period waves are typically reflected more than short period waves.

Dissipation

Dissipation of wave energy reduces or prevents overtopping without affecting conditions seaward of the wall. The principal mechanism by which wave energy is dissipated is through conversion into turbulence. Dissipation is increased by increasing the slope, porosity or roughness of the coastal defence. Sloped defences cause the waves to break, producing turbulence. Flatter slopes produce much more dissipation than steep slopes, with slopes of 1:1 or steeper performing roughly the same as vertical walls. Turbulence is induced in porous defences due to flow within the porous region. The porosity of the defence must decrease towards the wall or most of the wave energy will pass through and be reflected by the wall behind. Increasing the roughness of a wall creates turbulence by disrupting the flow.

Overtopping

Overtopping occurs in two forms: spray and green water. As waves break or impact the sea wall spray is produced and is carried past the defence by wind and the landward momentum of the wave. Dissipative coastal defences generally produce less spray than those which reflect wave energy.

Green water causes much more overtopping than spray. The height of a sea wall to which a wave reaches is known as the run-up. If this run-up exceeds the crest height green water overtopping occurs. To prevent this overtopping either run-up must be reduced through dissipation, or the crest height must be increased. Alternatively, on smooth or vertical walls, a recurve can be constructed at the crest to deflect run-up seaward.

2.2 Industry Practice

Two common methods to predict overtopping rates within industry utilise the Deltires Neural Network (NN) and the Eurotop Wave Overtopping of Sea Defences and Related Structures Assessment Manual. Both of these methods use data from the European CLASH database, a collection of laboratory experiments collected from various locations. Roughly 10,000 overtopping tests are represented in the database and each is described by various wave conditions and coastal defence configurations (van Gent et al., 2007). The NN uses 15 parameters to interpolate between data and predict overtopping rates (Coeveld et al., 2005). The NN is a very useful tool and is the primary overtopping prediction technique used by JBA consulting. However, if the input parameters fall outside the range of data then no prediction is made.

Eurotop utilises a different method to predict overtopping rates. Trend lines are fitted to data sets and then various equations are used to predict overtopping. Eurotop provides two possible overtopping predictions. Probabilistic design provides the absolute overtopping prediction and is used for forecasting purposes whereas deterministic design incorporates a factor of safety and is used for design purposes (EurOtop Manual, 2007).

3 Similitude

The aim of this investigation is to design an educational tool to demonstrate the performance of various coastal defences under a range of wave conditions.

When possible a geometrically undistorted model should be used as using a common scaling factor for all spacial dimensions generally produces a more accurate representation of flow characteristics.

When horizontal length scales are much larger than vertical length scales, as in many coastal engineering problems, restrictions on the size of the model often produce water depths of only a few tens of millimetres in geometrically undistorted models. At these water depths the affects of surface tension begin to dominate and capillary waves form (Komen et al., 1996), which greatly obscures results. This is the case for the wave tank being considered, and is compounded by the fact that the wave tank is to be used as a demonstration tool. A very shallow water depth does not allow easy visualisation of the fluid flows within the tank.

For these reasons a geometrically distorted model must be used for the wave tank. When using a distorted model care must be taken when analysing data. Flow properties may not be accurately represented so it is important to determine the degree of distortion, especially when there is a non-linear relationship between variables. There is also the potential for unknown scaling affects to influence the results (Hughes, 1993). However, no direct data comparison is made between full scale coastal conditions and the model so any discrepancies caused by geometric distortion are not of high importance.

3.1 Scaling

The water depth in the model is fixed at 70mm to avoid capillary waves and prevent water from splashing out of the tank. The wave height, wave length and period are chosen empirically to provide a good visual demonstration of how much overtopping occurs at each coastal defence. These values are then scaled upwards using a geometrically distorted scale and compared with wave data taken from monitor buoys at various locations on the British coastline.

When scaling between parameters in a prototype and a model a scaling factor, N , is found by

$$N_x = \frac{x_p}{x_m} \quad (1)$$

where x_p is the parameter in the prototype and x_m is the parameter in the model.

Hughes (1993) shows that geometrically distorted wave conditions can be scaled as follows:

The linear theory wavelength equation is used to produce the prototype-to-model ratio

$$\frac{[\lambda = \frac{gT^2}{2\pi} \tanh(\frac{2\pi h}{\lambda})]_p}{[\lambda = \frac{gT^2}{2\pi} \tanh(\frac{2\pi h}{\lambda})]_m} \quad (2)$$

or

$$\frac{\lambda_p}{\lambda_m} = \left(\frac{T_p}{T_m} \right)^2 \frac{\tanh\left(\frac{2\pi h_p}{\lambda_p}\right)}{\tanh\left(\frac{2\pi h_m}{\lambda_m}\right)}. \quad (3)$$

where

λ = wavelength

g = acceleration due to gravity

T = wave period

h = water depth

Expressed in terms of scaling factors, this becomes

$$N_\lambda = N_T^2 \frac{\tanh\left(\frac{N_h}{N_\lambda} \frac{2\pi h_m}{\lambda_m}\right)}{\tanh\left(\frac{2\pi h_m}{\lambda_m}\right)}. \quad (4)$$

Equation 4 shows that N_λ is a function of the model depth-to-wavelength ratio h_m/λ_m . If, however, we assume that wavelength is much larger than water depth then the tanh functions approach the value of their arguments and equation 4 becomes

$$N_\lambda = N_T^2 \cdot \frac{N_h}{N_\lambda} \quad (5)$$

which simplifies to

$$N_\lambda = \sqrt{N_h} \cdot N_T. \quad (6)$$

Equation 6 is used to determine typical real life wave conditions that are represented by those

in the wave tank.

In order to assess the reliability of these scaling factors, certain hydraulic criteria must be examined. This is commonly done using the Froude and Reynolds criteria. The density and viscosity of the prototype and model are similar whereas the length scales are vastly different meaning that Reynolds similitude is difficult to achieve.

This study uses a modified version of the Froude number to assess prototype-to-model similarity. The Froude number, Fr , relates the influence of inertial and gravity forces in a flow by:

$$Fr = \sqrt{\frac{\text{Inertial Forces}}{\text{Gravity Forces}}} = \sqrt{\frac{\rho L^2 U^2}{\rho L^3 g}} = \frac{U}{\sqrt{gL}} \quad (7)$$

where

ρ = fluid density

L = Length Scale

U = Fluid velocity

In the analysis of wave motion the fluid speed, U , is less important than the wave speed, c , so in the modified Froude number, U will be replaced with c and the wavelength will be used as the length scale to produce:

$$Fc = \frac{c}{\sqrt{gL}} \quad (8)$$

with wave speed calculated by:

$$c = \sqrt{\frac{g\lambda}{2\pi} \tanh \left(2\pi \frac{h}{\lambda} \right)}. \quad (9)$$

4 Experimental Procedure

Experiments are conducted in a rectangular tank of 200mm \times 183mm cross section and 1500mm length (figure 4). The results of this experimentation are used to inform the design of the demonstration wave tank. Following work by Goodfellow (2015), a rotary paddle wave maker is determined to be the most suitable wave maker design for this application. Figure 4 and table 1 detail the coastal defences and wave conditions that are investigated. For each combination of wave condition and coastal defence the experiment is run three times to ensure repeatability of the results. Further coastal defences and wave conditions are provided for use in the demonstration tank but are not considered in this study.

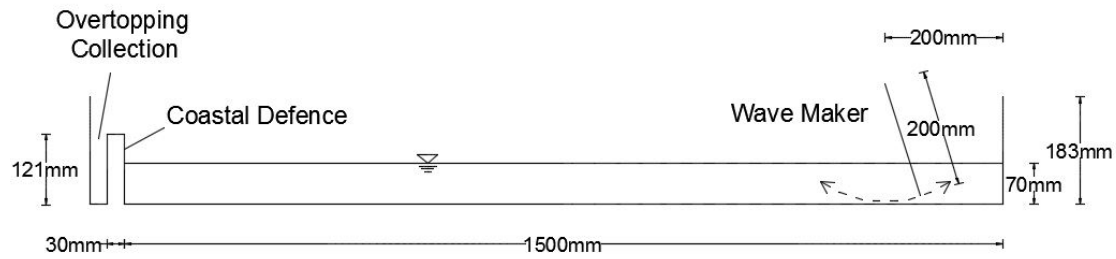


Figure 1: Wave tank

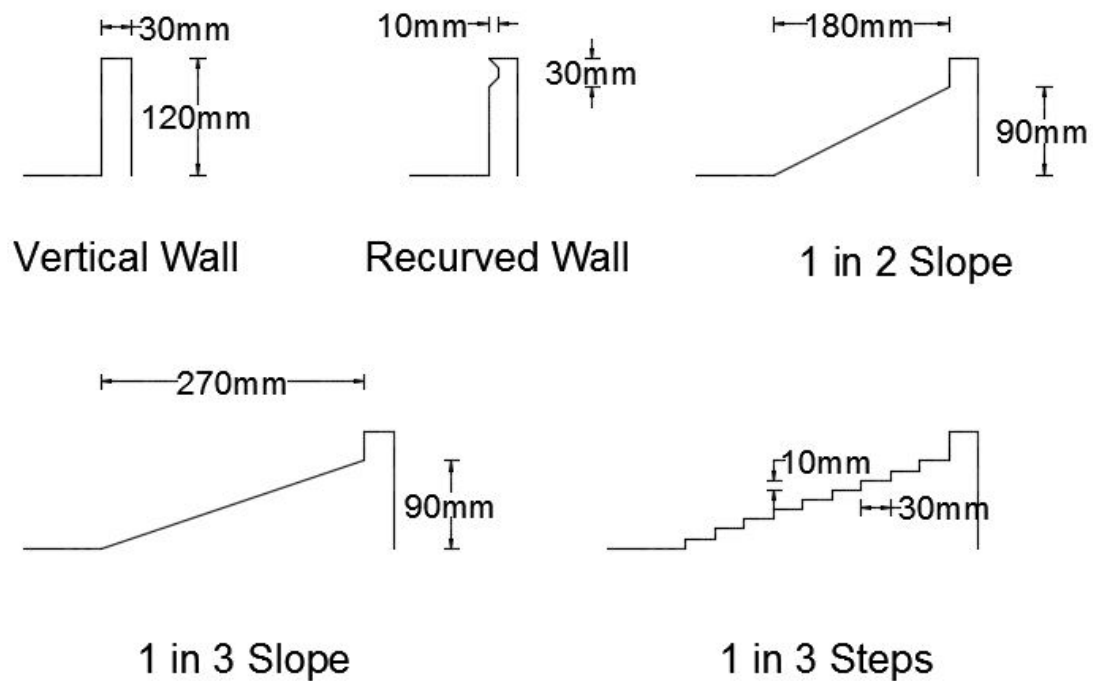


Figure 2: Coastal Defences Modelled Experimentally and Numerically

Continuous Wave Similitude

The continuous wave parameters are compared to the following wave conditions which occurred at Whitby on 15/08/2014:

- $h_p = 10.0\text{m}$
- $\lambda_p = 122.6\text{m}$
- $H_p = 3.42\text{m}$

- $T_p = 12.9\text{s}$

- $F_c = 0.274$

(Channel Coastal Observatory, 2015)

Using equation 1

$$N_\lambda = \frac{\lambda_p}{\lambda_m} = \frac{122.6}{1.005} = 121.99$$

which is in close agreement with equation 6:

$$N_\lambda = \sqrt{\frac{h_p}{h_m}} \cdot \frac{T_p}{T_m} = \sqrt{\frac{10.0}{0.07}} \cdot \frac{12.9}{1.25} = 123.35$$

The modified Froude numbers are also very similar showing that the continuous wave is a reasonable representation of the prototype wave conditions. Note that the same wave conditions are represented by the single wave.

Table 1: Experimental Wave Conditions

Wav	Wavelength, λ (m)	Wave Height, h (m)	Period, T (s)	F_c	Comments
Continuous	1.005	0.03	1.25	0.256	Waves are produced continuously for 15 periods to simulate wave impact on the coastal defence. A period of 1.25s is chosen as reflected waves impact the wave maker during its backwards stroke and are partially damped.
Solitary	1.005	0.03	N/A	0.256	A period of 1.25 does not completely damp out wave reflections so a single wave is used to assess overtopping without the affects of reflection.
Standing	0.650	0.02	0.84	0.306	A standing wave was tested on the vertical wall only to simulate resonant conditions which can occur in harbours.

Standing Wave Similitude

The standing wave parameters are compared to the following wave conditions which occurred at Bideford Bay on 11/22/2014:

- $h_p = 7.50\text{m}$

- $\lambda_p = 66.0\text{m}$

- $H_p = 5.6\text{m}$

- $T_p = 8.3\text{s}$

- $F_c = 0.312$

(Channel Coastal Observatory, 2015)

Using equation 1

$$N_\lambda = \frac{\lambda_p}{\lambda_m} = \frac{66.0}{0.650} = 101.54$$

which is in close agreement with equation 6:

$$N_\lambda = \sqrt{\frac{h_p}{h_m}} \cdot \frac{T_p}{T_m} = \sqrt{\frac{7.5}{0.07}} \cdot \frac{8.3}{0.84} = 102.28$$

The modified Froude numbers are also very similar showing that the standing wave is a reasonable representation of the prototype wave conditions.

Experimental Constants

Due to limitations in the experimental set up the following parameters remain constant:

- Water Depth - The depth of water in the experiments is kept constant at 70mm due to the restrictions on the dimensions of the tank. This water level avoids the capillary waves discussed in section 3 and allows adequate overtopping without spray leaving the tank. The water depth in the demonstration tank can be varied if required.
- Crest Height -The crest level is fixed at 120mm and is chosen based on the water depth of 70mm.
- Foreshore Slope and Level - The tank is level with an constant depth.
- Wave Direction - The wave tank is modelled as 2D with the approaching waves perpendicular to the width of the coastal defence.
- The affect of permeability on wave overtopping is not considered in this study.

4.1 Data Analysis

In each run the total volume of overtopping is collected, measured and converted into an overtopping rate in l/s. The flow in the tank is assumed to be 2D so position of the free surface is recorded as the water level at the wall of the tank. The free surface level is determined by analysis of images taken with a 1080 by 1920 pixel camera recording at 50 frames per second. To distinguish the position of the free surface there must be sufficient colour contrast between the fluid and the surrounding structures. To achieve this contrast the water is dyed black and the wave

maker, coastal defences and tank wall are coated with white backing plastic. For each video frame a reference distance is used to calculate the dimensions of a single pixel. Each pixel is converted to either black or white and this image is used to calculate the position of the free surface. This process is detailed in figure 4.1

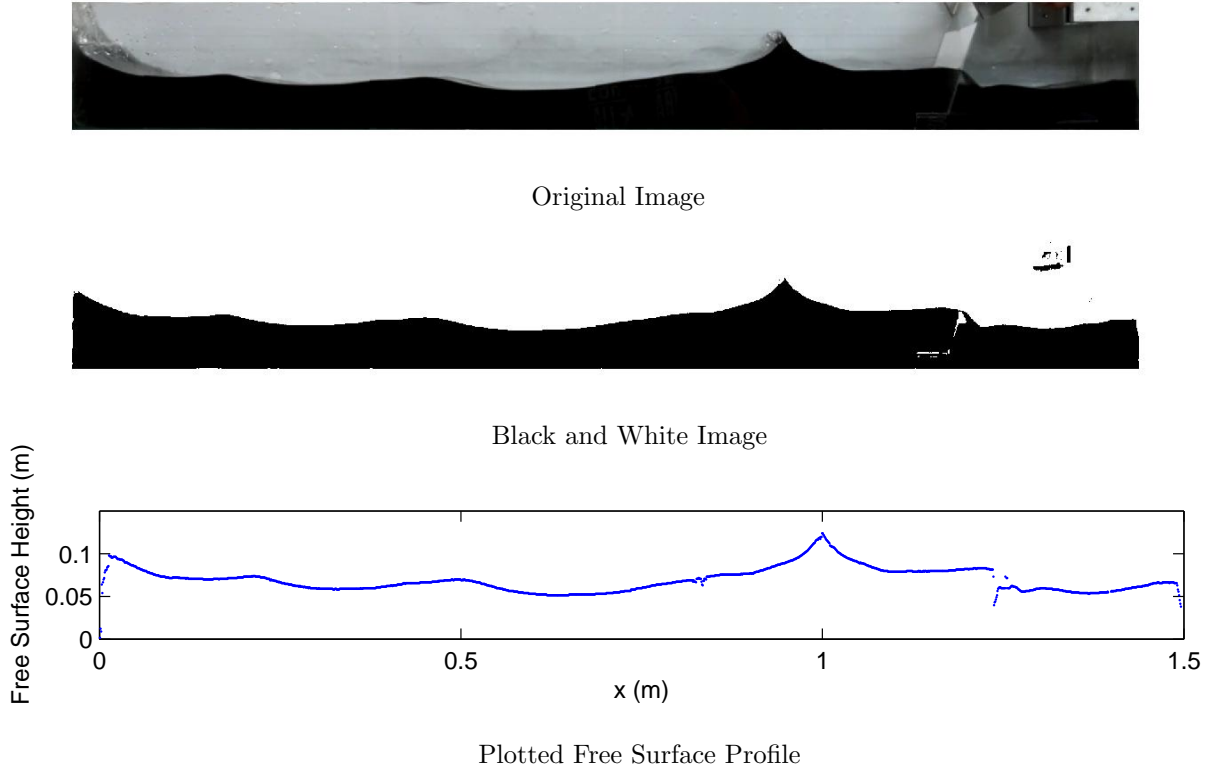


Figure 3: Image Analysis

4.2 Experimental Error

- A small volume of water leaks through the coastal defences and adds to the overtopping measurements. The amount of leakage is roughly 1.25ml/s in each case but is not consistent for each coastal defence.
- The coastal defences are constructed from foam to allow ease of construction and installation. Although the defences are secured to the base of the tank, buoyancy results in a small amount of uplift, slightly increasing the height of the defences. This is not the case for the vertical wall or the recurved walls as they were not submerged.
- The SPH simulation uses a stepped signal to define the velocity of the wave maker so there is no period of acceleration. The motion of the wave maker in the experiments is recorded using a rotary optical encoder. Figure 4 shows the rotation of the wavemaker over time for the continuous wave (Goodfellow, 2015). It can be seen that there is a small period of acceleration and deceleration at each change of velocity. Also, the forward stroke of the wavemaker is

sometimes resisted by reflected waves. Therefore the wavemaker does not always perform its full forward motion as it does in the SPH simulations.

- The SPH simulations are compared to the experimental results from the last frame where no motion is observable in the wave maker. As a result there is the possibility for the comparisons to be out of phase by one frame. However as the experiments are recorded at 50 frames per second, the maximum possible phase difference is 0.02 s.

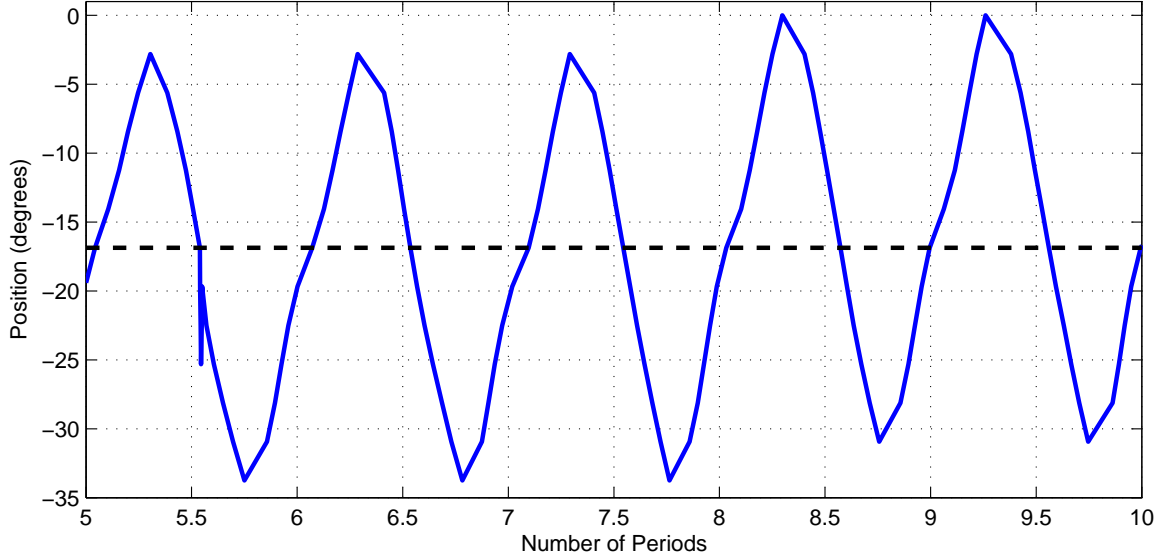


Figure 4: Rotation of Experimental Wave maker

5 Smoothed Particle Hydrodynamics (SPH) Theory

The wave tank is numerically modelled using the open source SPH software DualSPHysics. SPH is a Lagrangian numerical technique that was first developed by Gingold and Monaghan (1977) to model astrophysical problems. SPH models fluids as a set of particles rather than utilising a mesh based solver. This makes SPH particularly suitable for free surface problems as the free surface is directly simulated as the boundary between the fluid particles and the empty space, while other grid based numerical methods must track the free surface boundary.

By performing calculations according to particle position, rather than mesh nodes, computational work is only conducted in the important regions at any given time step rather than in empty areas as can be the case for mesh based solvers. However storing information of every particle becomes computationally expensive over time so SPH simulations can still have a considerable computational cost.

At each time step the properties of a particle are calculated by integration of the Navier-Stokes equations according to the physical characteristics of particles within a "smoothing length", h , of the particle in question. The hydrodynamic equations of motion for each particle are converted to appropriate form for particle based modelling using an integral interpolation function known

as the kernel function (W) (Barreiro et al., 2013). The kernel function approximates any function $F(\mathbf{r})$ by the integral approximation:

$$F(\mathbf{r}) = \int_{\Omega} F(\mathbf{r}') W(\mathbf{r} - \mathbf{r}', h) d\mathbf{r}'. \quad (10)$$

where \mathbf{r} is the vector position, W is the kernel function and Ω is the influence domain controlled by h . The function is then approximated in a discrete, non-continuous form. At particle a the function is interpolated over all particles within the smoothing length h ,

$$F(\mathbf{r}_a) \approx \sum_b F(\mathbf{r}_b) \frac{m_b}{\rho_b} W_{ab} \quad (11)$$

with h greater than the initial particle separation. In equation 11 m and ρ are the mass and density of particle b respectively. $W_{ab} = W(\mathbf{r}_a - \mathbf{r}_b, h)$ is the kernel function.

5.1 Smoothing Kernel

The choice of kernel function affects the performance of the SPH model and must satisfy the following conditions:

$$\text{Positivity: } W(\mathbf{r} - \mathbf{r}', h) \geq 0 \text{ inside the domain } \Omega, \quad (12)$$

$$\text{Compact support: } W(\mathbf{r} - \mathbf{r}', h) = 0 \text{ outside of the domain } \Omega, \quad (13)$$

$$\text{Normalisation: } \int_{\Omega} W(\mathbf{r} - \mathbf{r}', h) d\mathbf{r}' = 1. \quad (14)$$

w_{ab} must also monotonically decrease with increasing distance from a .

The accuracy of an SPH model generally increases with the order of the polynomials applied in the kernel function, as does the computational cost. Panizzo et al. (2007) found that the quintic, or Wendland, kernel:

$$W(\mathbf{r}, h) = \alpha_D \left(1 - \frac{q}{2}\right)^4 (2q + 1) \quad 0 \leq q \leq 2 \quad (15)$$

where $\alpha_D = 7/(4\pi h^2)$ in 2D has the best trade off between accuracy and computational cost. For this reason the Wendland kernel function has been chosen for all simulations in this study.

5.2 Compressibility

The standard SPH formulation treats the fluid as weakly compressible so requires an equation of state to calculate fluid pressure. This method has a much lower computational cost than solving equations used in the incompressible method, such as the Poissons equation. The DualSPHysics code uses Tait's equation of state:

$$P = B \left[\left(\frac{\rho}{\rho_0} \right)^\gamma - 1 \right] \quad (16)$$

to calculate the fluid pressure, P , according to work by Batchelor (2000). The parameter B is a constant related to the modulus of compressibility of the fluid, $\rho_0 = 1000 \text{ kg/m}^3$ is the reference density taken as the density at the free surface of the fluid and γ is the polytrophic constant which is typically between 1 and 7. Dumbser (2011) states that for water $\gamma = 7$ and is obtained by experimental fitting methods.

The speed of sound in the weakly compressible fluid is given by:

$$c^2(\rho) = \frac{\partial P}{\partial \rho} = \frac{B\gamma}{\rho_0} \left(\frac{\rho}{\rho_0} \right)^{\gamma-1} = \frac{B\gamma}{\rho_0^\gamma} \rho^{\gamma-1} \quad (17)$$

$$c_0^2 = c^2(\rho_0) = \left. \frac{\partial P}{\partial \rho} \right|_{\rho=\rho_0} = \frac{B\gamma}{\rho_0} \quad (18)$$

where c_0 is the speed of sound at the reference density and $B = c_0^2 \rho_0 / \gamma$. The value of B affects the speed of sound in the fluid and therefore the fluid's compressibility; choosing a value of B to give the real speed of sound would replicate incompressible flow. However, increasing the speed of sound significantly increases computational costs by reducing the time step of the simulation. The DualSPHysics software implements a variable time step which is dependent of the Corant condition, the force terms and the viscous diffusion term. The variable time step Δt is calculated by:

$$\Delta t = C \cdot \min(\Delta t_F, t_{CV}); \quad (19)$$

$$\Delta t_F = \min_a (\sqrt{h/f_a}); \quad (20)$$

$$\Delta t_{CV} = \min_a \frac{h}{c_s + \max_b \left| \frac{h v_{ab} x_{ab}}{r_{ab}^2} \right|}. \quad (21)$$

In equation 20 Δt_F is based on the force per unit mass $|f_a|$. In equation 21 Δt_{CV} controls the Courant condition and the viscosity and c_s is the speed of sound. It can be seen that a high speed of sound could result in very small time steps. (Monaghan, 1994) shows that provided that the speed of sound is at least ten times greater than the maximum expected fluid velocity, the speed of sound can be significantly reduced without affecting the fluid motion.

5.3 Viscosity Treatment

Two viscosity treatments are available in the DualSPHysics software; "artificial viscosity" and "laminar viscosity and Sub-Particle Scale (SPS)". Artificial viscosity utilises a parameter which must be calibrated for individual cases, whereas laminar viscosity with SPS aims to represent

the physical equations governing the system. In the DualSPHysics model the laminar viscosity and SPS viscosity treatment was utilised as this treatment has generally been shown to provide accurate results with less need for calibration (Crespo, 2008).

5.4 δ -SPH

In the DualSPHysics code a δ -SPH formulation can be introduced. This formulation applies a diffusive term to the continuity equation to reduce density fluctuations (Crespo et al., 2015). δ -SPH can be used to reduce numerical wave damping, however can also affect the compressibility of the fluid through changes in density. A δ -SPH of 0.1 is recommended for most applications but can be increased up to 1.0 if required (Crespo et al., 2015).

6 SPH Implementation Methodology

The previous chapter describes several factors that affect the SPH formulation. In order to ensure the accuracy of simulations, investigations into the affect of these parameters are conducted. This chapter summarises the findings of these investigations and further details are found in Appendix A. Details and findings of the simulations used in this investigation are detailed in table 2

Table 2: SPH Implementation Study Cases

Case N°	Particle Spacing d_p (mm)	N° of Particles	Aim	Description		Findings	
A1	1	105000	Particle Independence	Rotary Wave maker $T = 1s$ $H = 20mm$ $C_0 = 8.20 \text{ m/s}$		A2 and A3 show very good agreement up to 10T and good agreement at 20T. Observable change in volume caused by compressibility issues.	
A2	2	26250					
A3	5	4200					
A4	2	26250	Sound Speed Sensitivity Analysis	Tank with no wave maker	$C_0 = 8.20 \text{ m/s}$	Cases A4 and A6 produce significant variations in the free surface level, density and pressure. Case A5 shows only a small variation in these values.	
A5	2	26250			$C_0 = 20.50 \text{ m/s}$		
A6	2	26250			$C_0 = 32.81 \text{ m/s}$		
A7	2	26250	Sound Speed Sensitivity Analysis	Wave maker $T = 1s$ $H = 20mm$	$C_0 = 8.20 \text{ m/s}$	Cases A8 and A9 produce a sloped free surface at rest. Case A7 does not produce a sloped free surface but has a significant change in free surface level.	
A8	2	26250			$C_0 = 20.50 \text{ m/s}$		
A9	2	26250			$C_0 = 32.81 \text{ m/s}$		
A10	1	105000	Numerical Diffusion Analysis	Unforced Test Case $\delta\text{-SPH} = 0.1$ $C_0 = 20.50 \text{ m/s}$		Numerical diffusion damps out waves by 6 periods for all cases.	
A11	2	26250					
A12	5	4200					
A13	1	105000	Numerical Diffusion Analysis	Forced Test Case $\delta\text{-SPH} = 0.1$ $C_0 = 20.50 \text{ m/s}$		In each case waves are damped to approximately 50% of their original height across the domain	
A14	2	26250					
A15	5	4200					
A16	2	26250	Numerical Diffusion Analysis	Unforced Test Case	$\delta\text{-SPH} = 1.0$	Increasing $\delta\text{-SPH}$ slightly reduces damping rate but causes an increase in fluid volume	
A17	2	26250			$\delta\text{-SPH} = 0.5$		
A18	2	26250			$\delta\text{-SPH} = 0.1$		
A19	2	26250	Numerical Diffusion Analysis	Forced Test case	$\delta\text{-SPH} = 1.0$	$\delta\text{-SPH}$ value of 1.0 results in waves damping to roughly 70% of their original height but a change in fluid volume is also observed	
A20	2	26250			$\delta\text{-SPH} = 0.5$		
A21	2	26250			$\delta\text{-SPH} = 0.1$		
A22	1	105000	Particle Independence	Rotary Wave maker $T = 1s$ $H = 20mm$ $C_0 = 20.50 \text{ m/s}$ $\delta\text{-SPH} = 1.0$		Cases A22 and A23 show good agreement at 10T and reasonable agreement at 20T.	
A23	2	26250					
A24	5	4200					

6.1 Initial Particle Independence Study

An initial particle independence study is conducted to assess the affect that particle spacing has on the simulations and determine an appropriate initial particle spacing to use. The wave tank is modelled with a rotary paddle wave maker using three values of d_p , 1mm (Case A1), 2mm (Case A2) and 5mm (Case A3).

This particle independence study shows that cases A1 and A2 produce very similar results after 10 periods and good agreement after 20 periods the results are still reasonably similar. The study also shows that the volume of fluid in the simulations changes by up to 8.9%, this is analysed in more detail in section 6.2.

6.2 Sound Speed Sensitivity Analysis

The particle independence study discussed in section A.1 finds that the volume of fluid in the simulations changes, showing compressible behaviour of the fluid. The DualSPHysics code treats the fluid as weakly compressible and relates the speed of sound in the simulation to density and pressure with equations 16 and 18.

Cases A1, A2 and A3 have a speed of sound of 8.05 m/s with maximum fluid velocity of 0.7 m/s. According to (Monaghan, 1994) this value of C_0 should not affect the fluid as it is greater than ten times the maximum fluid speed, however, this is not the case. Sensitivity analysis is conducted in order to determine an appropriate speed of sound to produce a constant fluid volume in the wave tank with an acceptable computational cost.

Simulations are conducted in a 1.5m long rectangular tank with no wave maker to assess the volume change with no energy input. Sufficient time is allowed for each simulation to come to rest.

The simulations show that lower speeds of sound caused an increase in the fluid volume whereas higher speeds of sound cause a decrease in fluid volume and require significant computational time. Increasing the speed of sound also causes the free surface to become sloped, with a maximum angle of 0.172° observed for $c_0 = 32.19\text{m/s}$. It is unclear why this is. A sound speed of 20.12m/s results in a minimal change in volume and only a small slope of the free surface.

The recorded pressures and densities at the midpoint of the tank are compared to analytical values derived by Goodfellow (2015). The lower speed of sound produces an increase in volume and also an increase in the pressure and density. Similarly, the higher speed of sound produces a reduction in volume, pressure and density. The reasons for this are discussed in Appendix A.2. A speed of sound of 20.12m/s produced relatively constant values of pressure and density.

Simulations are also conducted in the same tank with a rotary wave maker. The wave period is one second and the wave height is 10mm. The wave maker runs for 40s and the simulation continues for a further 20s to allow the fluid to come to rest. The results are very similar to those of the tank with no wave maker and the same conclusions can be drawn.

The results of the sound speed sensitivity analysis show that $c_0 = 20.12\text{m/s}$ produces the smallest change in volume, pressure and density. At this speed of sound a the slope of the free

surface was relatively small and is considered preferable to the larger volume change produced with a lower speed of sound. The computational time of this speed of sound is also considerably less than for $c_0 = 32.19$ m/s.

6.3 Test Cases

SPH has been shown to accurately simulate the interaction between waves and structures in many studies including Gómez-Gesteira and Dalrymple (2004) and Altomare et al. (2014). However, numerical diffusion in the formulation is known to produce artificial damping of propagating waves.

The SPH model is compared to analytical test cases in order to assess the accuracy of wave propagation in the SPH formulation and determine whether adjustment of the model is required to accurately simulate the specified wave conditions.

In the simulations the viscosity value, which corresponds to the kinematic viscosity of the fluid, is set to 0 so that no physical damping occurs in the system and the numerical diffusion can be accurately assessed.

6.3.1 Unforced Case

Goodfellow (2015) derives an expression for the free surface level of an unforced standing wave varying with time. The analytical solution of a standing wave with $\lambda = 0.75$ m is compared to SPH simulations of varying particle spacing in order to assess numerical diffusion in the system.

In order to set up an unforced standing wave in DualSPHysics the initial conditions of the fluid must be set. At time, t , the velocity of the fluid is defined as a function of location, however, in the DualSPHysics software the initial velocity can only be imposed as a vector for the entire fluid. It is possible, however, to specify the starting position of the fluid particles. At $t = 0$, $t = T/2$ and $t = T$ the kinetic energy of the standing wave is at its maximum, whereas the potential energy is at its minimum. At $t = T/4$ and $t = 3T/4$ potential energy is at its maximum, with the standing wave reaching its maximum height. At these times the kinetic energy is zero so the properties of the fluid can be modelled in DualSPHysics to create a standing wave.

The position of the free-surface at $t = T/4$ is calculated, and the profile of the fluid modelled using 3D modelling software to create a .stl file. This file is then imported into the DualSPHysics software and scaled to fit the domain, producing the required standing wave. As there is no viscosity in the system, the standing wave that is produced should continue with the same amplitude indefinitely. Any reduction in the height of the wave is therefore due to numerical diffusion.

6.3.2 Forced Case

The analytical solution of the unforced standing wave is modified by Goodfellow (2015) and Booker (2015) to introduce a repeated energy input into the system by means of a moving boundary.

As the energy of the fluid is transferred from an external input, no initial fluid conditions are required. In the DualSPHysics simulation the fluid begins at rest and one wall oscillates with a sinusoidal motion to instigate the standing wave.

For a specified wave number, k , the angular frequency of the wave, ω , was determined using the dispersion relation

$$\omega^2 = gk \tanh(kH).$$

The linear frequency, f , of the moving wall was then calculated by

$$f = \omega/2\pi.$$

A small amplitude of 0.1m is chosen so that there is not a large change in the length of the domain, preventing the standing wave from becoming out of phase. A wave number, k , of 6π is chosen, creating a wavelength, λ of 0.67m.

Test Cases Summary

The test cases show that significant numerical damping occurs in the SPH simulations. The unforced standing wave energy is almost completely damped after six periods and the forced waves are damped to roughly 50% of their initial height over the length of the 1.5m wave tank. Diffusion rates do not appear to be greatly affected by particle spacing.

Due to the significant numerical damping observed in the simulations, further study is conducted into the effect of varying the parameter δ -SPH from its default value of 0.1. The same test cases are simulated with a constant particle spacing of 2mm and values of δ -SPH of 0.1, 90.5 and 1.0.

Again the unforced test cases reach their lowest potential energy after around six periods, with a slightly lower dissipation rate occurring for larger values of δ -SPH. Increasing the value of δ -SPH also causes the fluid volume to increase up to a maximum of 2.8%. This shows that increasing the value of δ -SPH above its recommended value of 0.1 produces density variations described by Crespo et al. (2015).

The forced test case showed that increasing the value of δ -SPH to its maximum of 1.0 resulted in the waves damping to roughly 70% of their original height over the length of the wave tank. Although the numerical diffusion is reduced, large fluctuations in the fluid volume are produced. In section 7.1 varying values of δ -SPH are compared with experimental data to establish an appropriate value for the simulations.

6.4 Revised Particle Independence Study

The initial particle independence study is repeated using a revised speed of sound of 20.12 m/s. The study finds that cases A22 and A23 show very good agreement after 10 periods and reasonable agreement after 20 periods.

6.5 Conclusions of SPH Implementation Studies

Several variables in the SPH formulation are investigated. From the results of this investigation it is decided that an initial particle spacing of 2mm combined with a sound speed of 20.12 m/s is appropriate for simulation of the wave tank. This combination of parameters provides reasonable particle independence and only small variations in fluid volume, pressure and density. Comparisons with experimental data are made in section 7 to determine an suitable value of δ -SPH.

7 Results

The experimental overtopping measurements of the coastal defences studied are compared to establish the performance of each defence. The experimental overtopping is are then compared to the overtopping of the SPH simulations. The free surface profile of SPH simulations are also compared to the experimental data.

7.1 Repeatability

Figure 5 shows the three repetitions of the continuous wave impacting the vertical wall at $t=17.8s$. It can be seen that the free surface profiles are very similar close to the maximum time of the experiment. Similar agreement is shown for all of the coastal defences so the experimental data can be considered reliable.

The experimental results also shows some anomalous data from the image processing results behind the wave maker. This is due to the image processing software as the stand which supports the wave wave maker causes shading in this area. The free surface height in this area, however, is not the focus of this study so the anomalous data is of little importance.

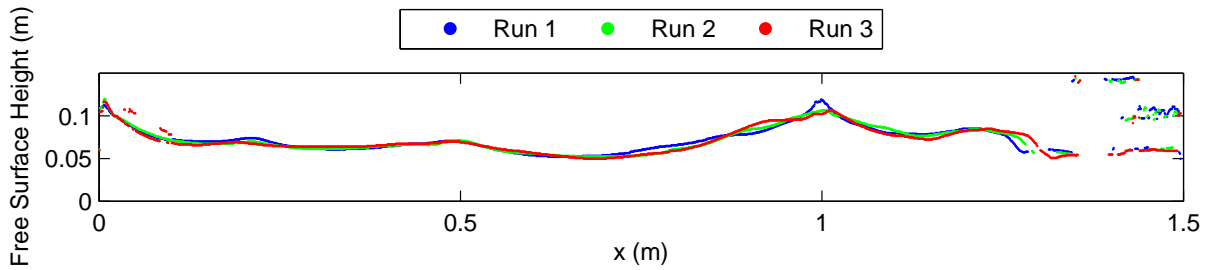


Figure 5: Free Surface Profiles of three separate experimental runs at $t=17.8s$

7.2 Experimental Wave Overtopping

Table 3 shows the total volume of water overtopped for each of the coastal defences subjected to the continuous and single waves. There is considerably less overtopping of the recurred wall and stepped slope than the other coastal defences. Figure 6 shows the single wave impacting each coastal defence. The wave only runs part way up the steps and does not quite reach the topmost step. This is due to high rates of energy dissipation across the steps. The wave runs up the recurred

wall to approximately the same level as the vertical wall. However, there is little overtopping as green water is reflected backwards away from the defence.

This shows that these coastal defences are efficient and preventing overtopping but use different methods. The Recurved wall reflects wave energy seaward whereas the steps dissipate the wave energy.

Table 3: Experimental Overtopping

Coastal Defence	Mean Overtopping of Single Wave (ml)	Mean Overtopping of Continuous Wave (ml)
Vertical Wall	70	502
Recurved Wall	<5	48
1:2 Slope	74	415
1:3 Slope	67	431
Stepped Slope	<5	48

The vertical wall, 1 in 2 slope and 1 in 3 slope all produce similar volumes of overtopping when subject to a single wave. It is expected that an increase in slope would reduce overtopping. A possible reason for the similar levels of overtopping may be that the depth of water is too high for the slopes to be effective. A higher water depth reduces the length of the slope over which waves can run up and be dissipated. It can be seen from figure 6 that there is a much greater amount of green water overtopping the two slopes than the vertical wall. The slopes are acting as a ramp for the wave energy so more water is overtopped.

After 15 periods the total overtopping is much less than 15 times the overtopping of a single wave. The reason for this is that wave energy is reflected by the coastal defence and interacts with approaching waves, causing them to break. These approaching waves then have less energy so cause less overtopping. This highlights how the wave action seaward of the coastal defence can be significantly increased by wave reflection. Dissipation should therefore be considered in sea wall design in order to reduce this affect.

The vertical wall reflects more wave energy than the sloped defences so it would be expected that this would cause more wave breaking and reduce the total overtopping after 15 periods. However the sloped coastal defences result in noticeably less overtopping than the vertical wall after 15 periods. A possible reason for this is once the approaching waves have broken, the wave energy has reduced sufficiently for the slopes to dissipate energy efficiently.

Contrary to what would be expected the 1:3 slope produces slightly more overtopping than 1:2 slope. This may be due to the fact that the 1:2 slope reflects more wave energy, increasing the breaking of the approaching waves.

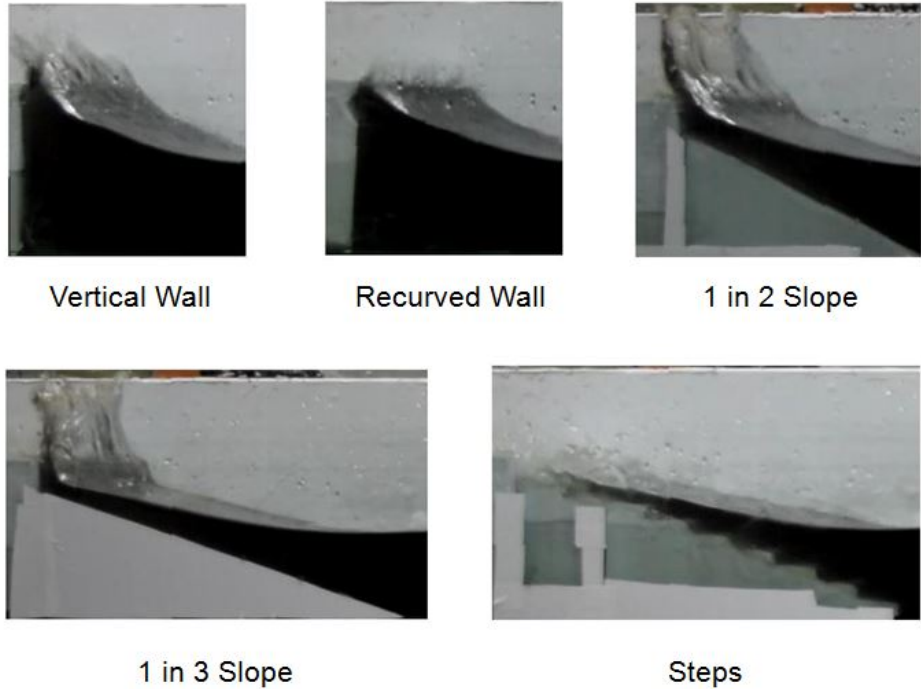


Figure 6: Images of Overtopping for Each Coastal Defence

7.3 Determination of δ -SPH

The free surface profile of the continuous wave acting on the vertical wall is compared to SPH simulations using values of δ -SPH of 0.1 and 1.0. Figure 7 shows that at $t=2.7\text{s}$, when the first wave impacts the wall, the SPH simulations both show good agreement with the experimental data. At $t=11.5\text{s}$ (figure 8) the experimental data shows a breaking wave at $x=1.0\text{m}$. Comparing this to the two SPH simulations, δ -SPH = 0.1 shows the wave breaking whereas δ -SPH = 1.0 does not. Figure 7.3 shows visualisations of the two simulations at $t=11.5\text{s}$. it can bee seen that for δ -SPH = 0.1 the measured free surface level closely matches the positions of the topmost fluid particles. For δ -SPH = 1.0, however, there is a distinct disparity in the level of the fluid particles and the measured free surface. This is due to the destiny fluctuations highlighted in section 6.

It can be seen that the fluid particles demonstrate the wave breaking, however these particles are above the recorded free surface level so the wave breaking does not appear in the free surface measurement. Figure 8 also shows that the collected overtopping is not recorded by the free surface measurement with δ -SPH = 1.0. Other than the wave breaking the free surface measurements of the free surface profile of both simulations closely match the experimental data and the numerical damping predicted in section 6.3 is not apparent. It is unclear why this is, however it may be due to the viscosity in the simulations outweighing the numerical diffusion. Further simulations use a value of δ -SPH of 0.1 as this value produces a more accurate prediction of the free surface profile.

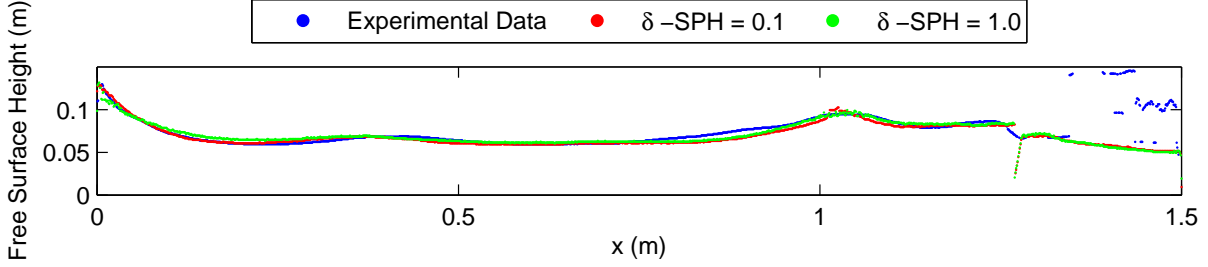


Figure 7: Free Surface Profiles of Experimentation and SPH Simulations with Varying δ -SPH Values at $t=2.7\text{s}$

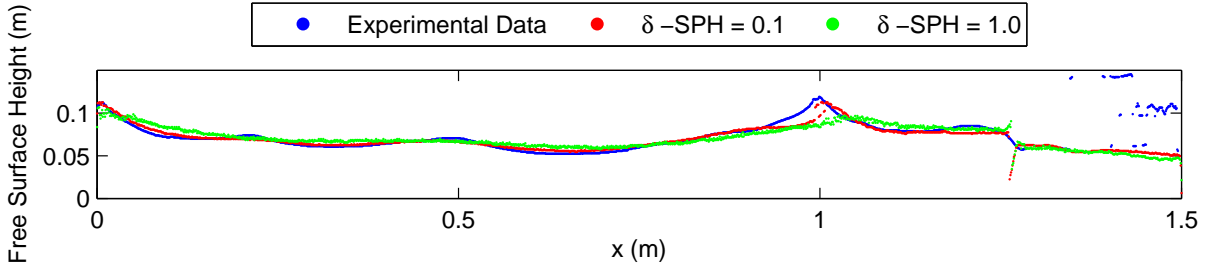


Figure 8: Free Surface Profiles of Experimentation and SPH Simulations with Varying δ -SPH Values at $t=11.5\text{s}$

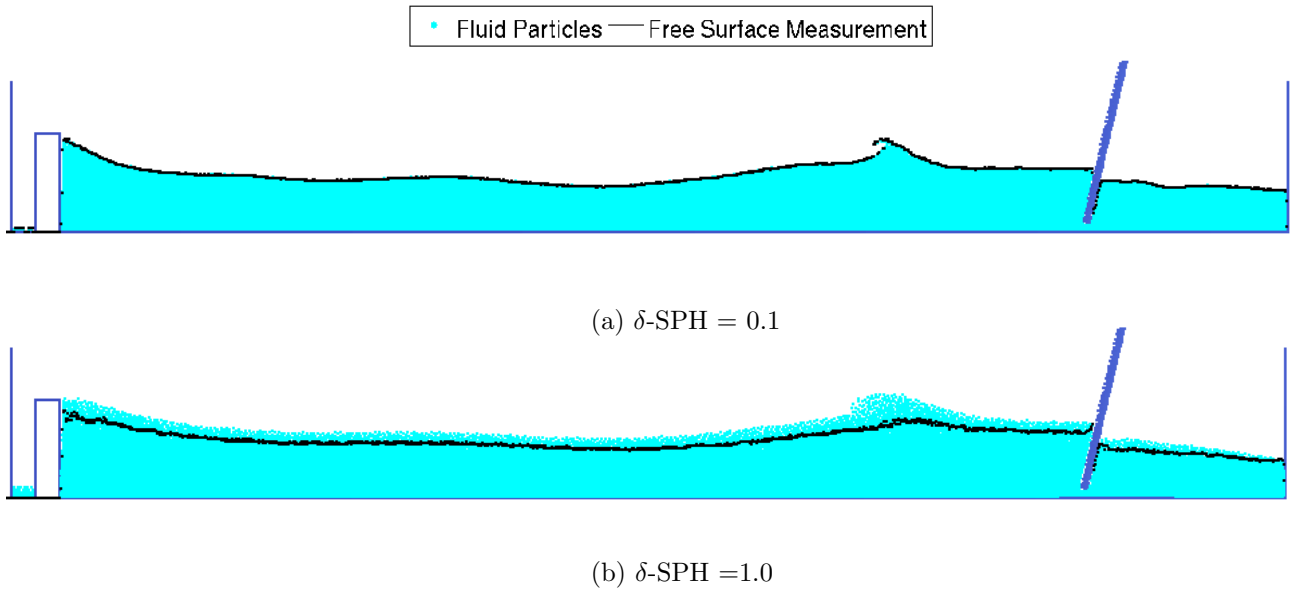


Figure 9: SPH Visualisations of (a) δ -SPH = 0.1 and (b) δ -SPH = 1.0 at $t=11.5\text{s}$

7.4 Continuous Waves

The free surface profiles of all of the simulations show good agreement with the experimental data, with the similarity deteriorating slightly over time. Figure 10 shows the stepped slope at $t = 2.7\text{s}$ when the first wave impacts the crest of the wall. The two profiles match extremely well, however some wave breaking is apparent in the SPH simulation at $x=1\text{m}$ that does not occur in

the experimental data. Note that towards the crest of the wall the experimental data shows a free surface height of 0m. This is due to splashing of the water reducing the contrast of the image at this time. This makes it difficult for the image processing software to identify the free surface level. This splashing is seen in the SPH simulation.

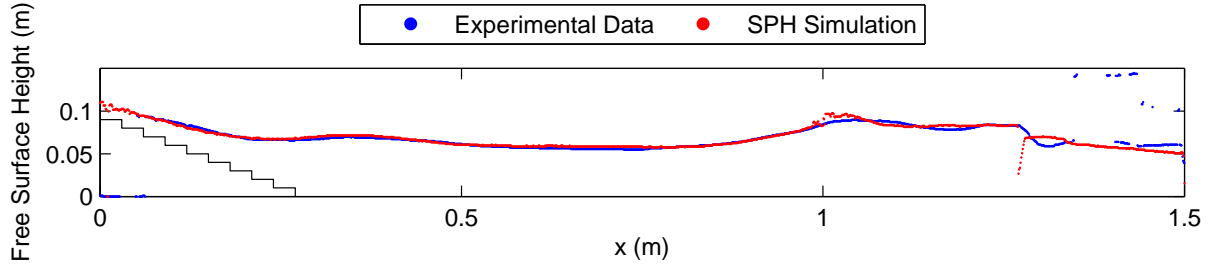


Figure 10: Free Surface Profiles of Experimentation and SPH Simulation at $t=2.7\text{s}$

Figure 11 shows the 1 in 3 slope at $t=11.5\text{s}$. There is reasonably good agreement between the experimental data and the SPH simulation and the wave run up is at approximately the same position. At $x=1\text{m}$ there is again wave breaking in the SPH simulation that is not observable in the experimental data. The crest of the breaking wave is also slight behind that of the experimental data. While the simulation shows the same general level of the free surface, the profile is much smoother than the experimental data. Small, low energy waves which occur in the experiment are not predicted by the simulation. This is likely due to the effects of numerical diffusion discussed in section 6.3, however the viscosity value used may also affect the results.

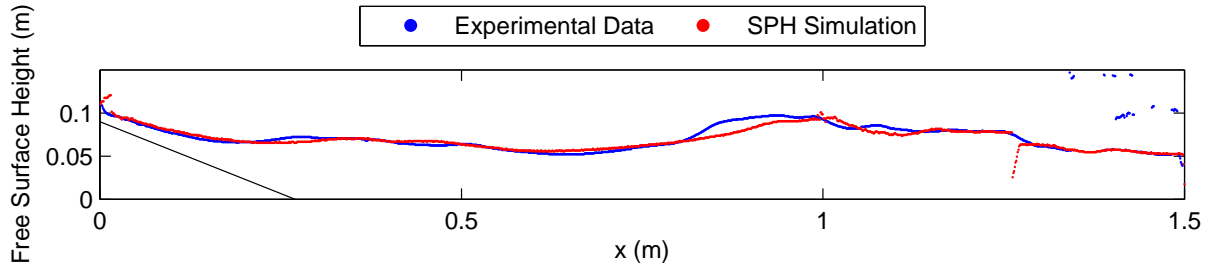


Figure 11: Free Surface Profiles of Experimentation and SPH Simulation at $t=11.5\text{s}$

Figure 12 shows the vertical wall at $t=17.8\text{s}$, close to the maximum time of the experiment. Again there is a good general agreement of the profile of the free surface and the the level of wave run up. The breaking wave at $x=1\text{m}$ is apparent in both cases, with the SPH simulation slightly under estimating the height of the wave breaking. The small waves visible in the experimental data are again damped in the simulation.

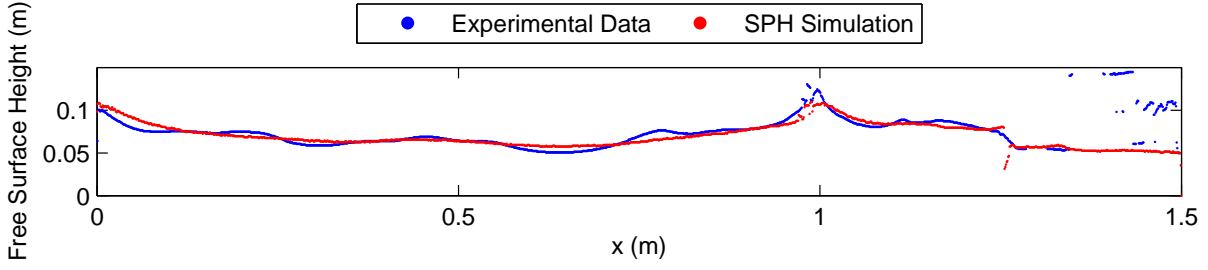


Figure 12: Free Surface Profiles of Experimentation and SPH Simulation at $t=17.8s$

Figure 13 show the steps at the same value of t . Here the small waves are not present in the experimental data and the two profiles are in better agreement. This is because the small waves are caused by reflection of the wave energy. As a most of the wave energy is dissipated by the steps there is little reflection so the smaller waves do not occur. This again highlights the importance of energy dissipation at a coastal defence to reduce wave action seaward of the wall.

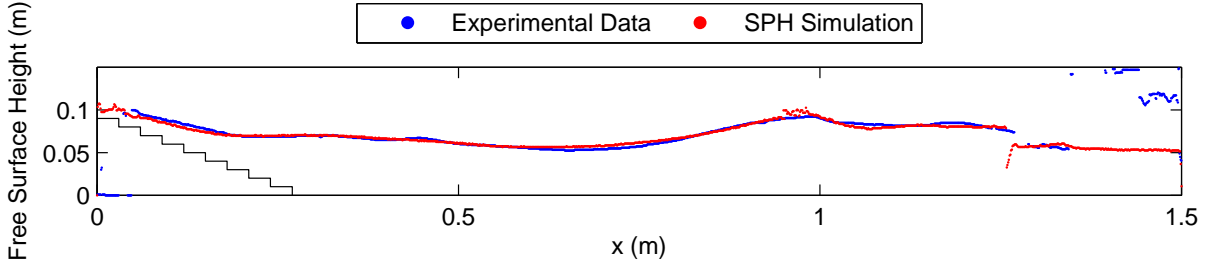


Figure 13: Free Surface Profiles of Experimentation and SPH Simulation at $t=17.8s$

Figure 14 shows the free surface height at $x=0.75m$ for the vertical wall over time. It can be seen that there are significant variations in the free surface level between the experimental data and the simulation. This is due to wave reflections causing a disordered fluid motion that is not accurately simulated by the SPH model. However, a general trend of periodic oscillations can still be seen. The two plots are reasonably in phase with one another initially but a small phase difference is observed at higher values of t .

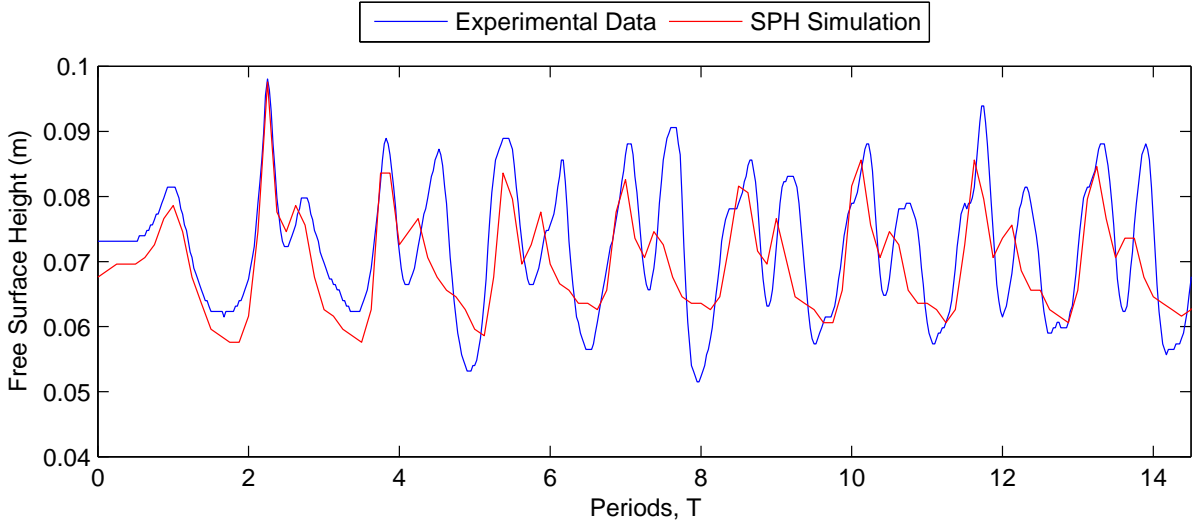


Figure 14: Free Surface Height of Experimentation and SPH Simulation at $x=0.75\text{m}$

Figure 15 shows the same data for the stepped coastal defence. In this case there is far less wave reflection due to energy dissipation on the steps. This produces a re more regular fluid motion which is more accurately simulated by the SPH model. In this case there is a smaller phase difference between the experiment and the simulation as time increases.

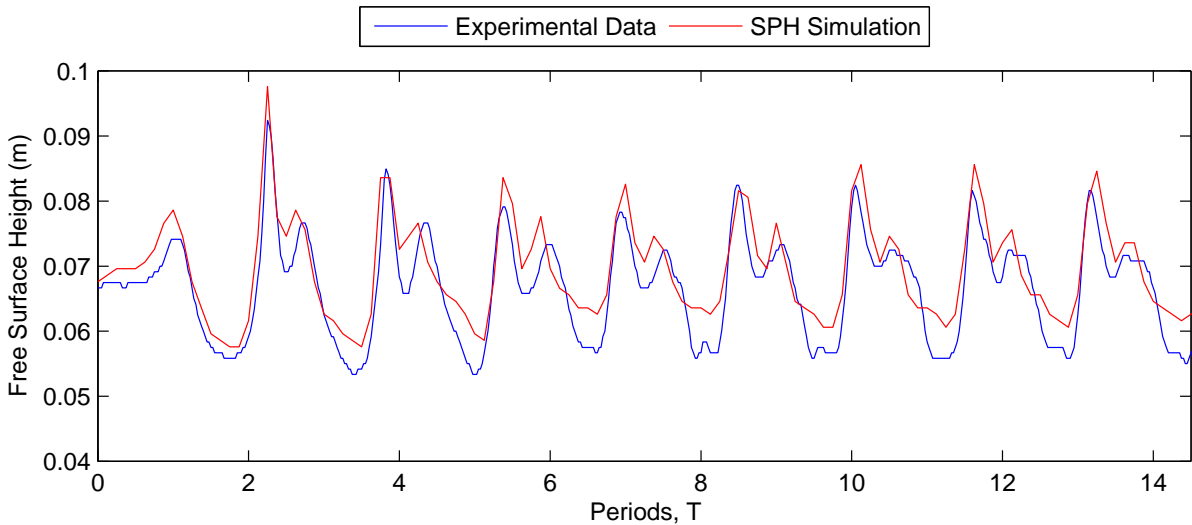


Figure 15: Free Surface Height of Experimentation and SPH Simulation at $x=0.75\text{m}$

Further comparison of the SPH simulations and experimental results are found in Appendix B. For each coastal defence there is roughly the same agreement between the experimental results and the simulations.

7.5 Single Wave

Figure 16 shows the recurved wall at $t=2.7\text{s}$ as the single wave impacts the defence. Like in the continuous cases there is very close agreement between the experimental data and the simulation.

Figure 17 shows the recurved wall at $t=4.0\text{s}$ as reflected waves are dissipating. There is still close agreement between the plots, however the numerical diffusion of the SPH simulation is observable.

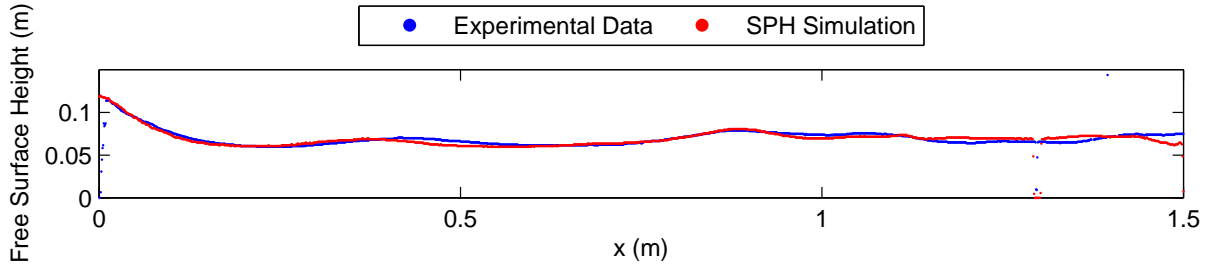


Figure 16: Free Surface Profiles of Experimentation and SPH Simulation at $t=2.7\text{s}$

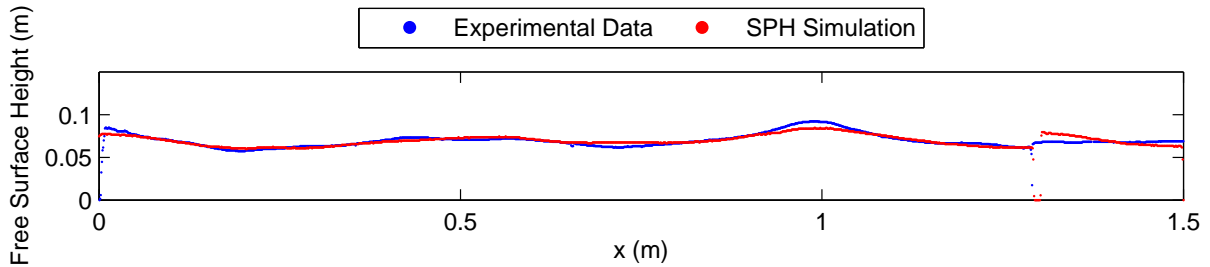


Figure 17: Free Surface Profiles of Experimentation and SPH Simulation at $t=4.0\text{s}$

7.6 Standing Wave

Figure 7.6 shows the standing wave at increasing values of t . It can be seen that the height of the standing wave grows due to resonance. At $t=9.6\text{s}$ (roughly 11 periods) the waves reach their full height and do not increase further by 13.8s . This shows how waves entering a harbour with a frequency close to the resonant frequency of the harbour can quickly increase in amplitude. This can cause unsafe conditions for ships and boats.

The SPH simulations closely match the experimental data in all cases. The peak of the standing wave at $x=1.0\text{m}$ is slightly lower and has travelled slightly further in the SPH simulation at all values of t . However by the time the waves have reached the second peak at $x=0.3\text{m}$ the experimental data and SPH simulation match more closely.

Figure 7.6 (a) shows that the profile of the waves in the SPH simulation is smoother than the experimental data. This demonstrates the numerical diffusion in the simulation.

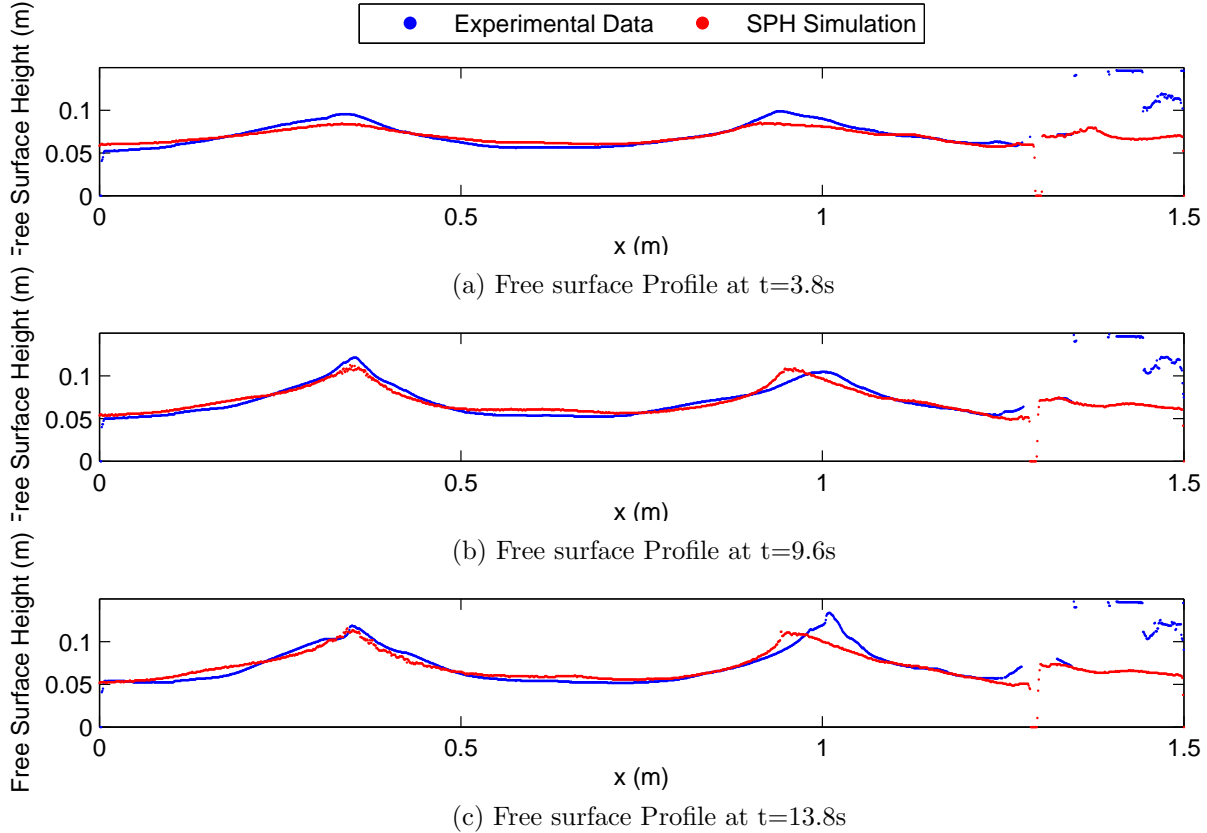


Figure 18: Development of Standing Wave

7.7 Simulated Wave Overtopping

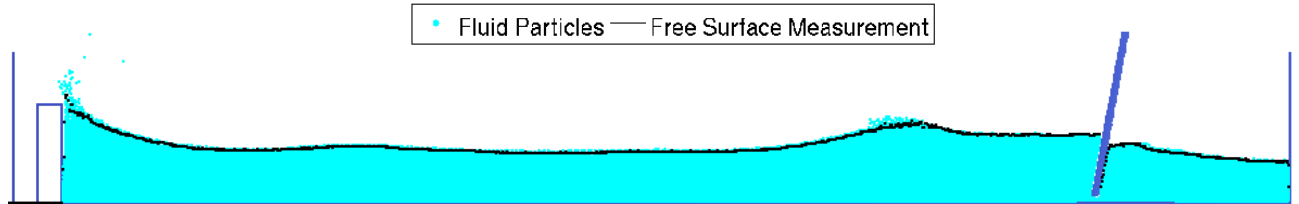
Table 4 shows the overtopping measured by the SPH simulations. In all cases the overtopping is only considerably less than the experimental measurements. In the experiments a small volume of water leaked through the coastal defence and added to the measured overtopping, however even with this considered the the SPH simulations significantly underestimate overtopping. Figure 7.7 shows the SPH visualisation and an image of the first wave impacting the vertical wall. In the experiment most of the overtopping occurs as green water whereas in the SPH simulation it mostly occurs as spray.

Table 4: Simulated Overtopping

Coastal Defence	Mean Overtopping of Single Wave (ml)	Mean Overtopping of Continuous Wave (ml)
Vertical Wall	17.6	26.5
Recurved Wall	6.42	24.8
1:2 Slope	8.8	0
1:3 Slope	5.8	0
Stepped Slope	0	0



(a) Experiment



(b) SPH Simulation

Figure 19: Comparison of the Forms of Overtopping Between Experimentation and SPH simulation t=11.5s

There are several possible reasons for the difference in the form of overtopping between the experiment and simulation.

- The Laminar Viscosity + SPS viscosity treatment is used in the simulations with the viscosity value set as the kinematic viscosity of water. This value is assumed to be correct, however is not verified. The temperature of the water in the experiment was not recorded so the kinematic viscosity value used could be incorrect. If the viscosity in the simulation is too low then the fluid is more likely to break up into droplets rather than remain as a continuous body. Further investigation should be conducted to ascertain an appropriate viscosity value to use.
- The particle spacing may be too coarse to accurately represent the fluid motion as it overtops the wall. Increasing the particle spacing further may remedy this problem but would also increase computational time.
- Numerical diffusion reduces the wave energy impacting the defence so that it is splashed upwards rather than flowing directly over the wall.

Both the 1:2 slope and the 1:3 slope produced no overtopping under the continuous wave conditions but produced small amounts of overtopping after the single wave. This is unusual as the wave parameters are identical in both cases until after one full period at t=1.875s. The only possible explanation for the differences in overtopping is that as the wave maker continues to move in the continuous cases, it alters the wave profile sufficiently to prevent overtopping from occurring.

8 Insert and Tank Design

The results of this investigation help to inform the final design of the demonstration tank. In order to ensure the tank is fit for purpose the following properties are incorporated into the design:

- The tank must be easily transportable so its dimensions are restricted to 1500mm length × 200mm width × 183mm height.
- The volume of overtopping must be clearly demonstrated. The tank is raised by 100mm and a tap is placed in the overtopping collection chamber. This allows overtopped water to be easily drained into a suitable container.
- The tank is to be used in a wide range of locations where a level surface may not always be present. Therefore the tank sits on adjustable levelling feet. Two bubble levels are fitted in the x and y axes so that the feet can be adjusted to ensure that the tank is horizontal. The levelling feet are fixed to a removable stand on which the tank sits. This allows the tank to be dismantled for ease of transport.
- As water is overtopped the water depth in the tank is reduced. A removable hopper with a volume scale is attached above the tank, close to the wave maker. There is also a volume scale in the collection chamber. The volume of water lost through overtopping can therefore be added back into the tank between each demonstration.
- A depth scale is placed in the tank. This allows demonstrations with measurable differences in water depth to be conducted.
- The control system for the wave maker sits in a perspex housing. This protects electronics from water and allows the wave maker to be easily controlled. The wave maker and control system housing are also detachable for ease of transport. The design of the wavemaker is discussed further by Goodfellow (2015).

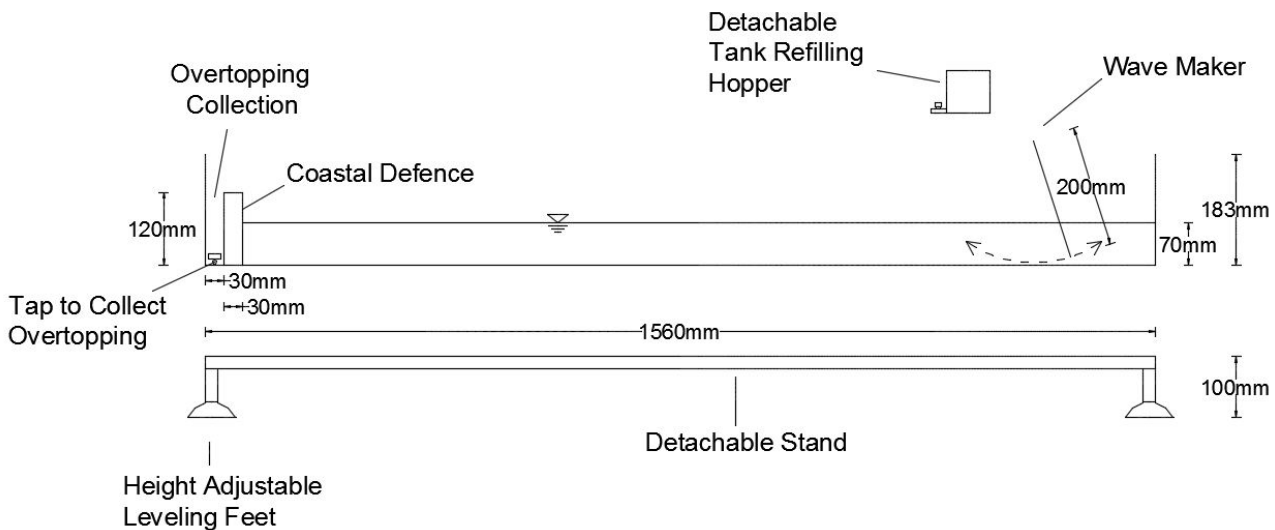


Figure 20: Final Tank Design

Figure 21 shows the additional coastal defences that are available with the demonstration tank. Each insert is easily clipped in and out of the tank. The seawall is permanently fixed into position to a height of 90mm to form a water tight barrier. A 30mm vertical or recurred wall is then inserted into the top of fixed wall. Horizontal spacers can be used in conjunction with any coastal defence to demonstrate how varying the horizontal length of a sea wall affects overtopping. An offshore breakwater can also be inserted at the midpoint of the tank. Further defence types can be easily specified to order if required by JBA for future projects.

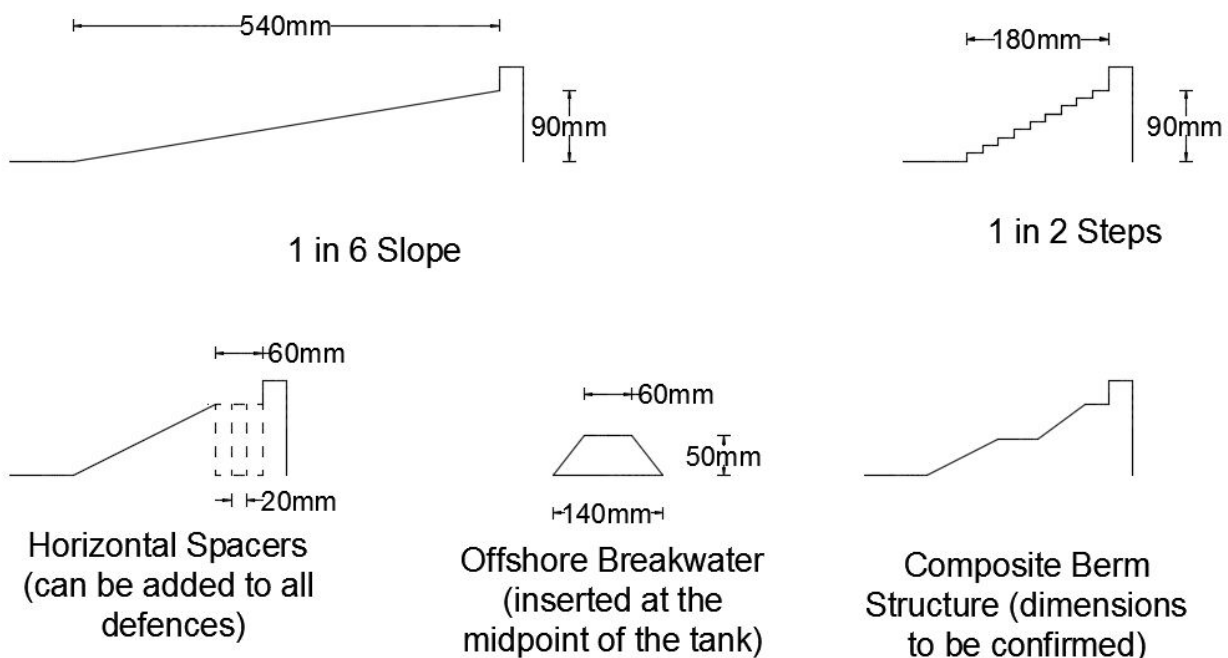


Figure 21: Additional Coastal Defences

9 Conclusions

Experiments conducted in a model wave tank show how various coastal defences affect wave overtopping. Minimal overtopping occurs for the stepped slope and recurved wall. This highlights how dissipation and deflection of wave energy are highly effective methods of preventing overtopping.

For a single wave the sloped defences result in a similar amount of overtopping as the vertical wall. This is because a high water depth causes an insufficient run up length for dissipation to occur. After 15 wave periods the slopes produce less overtopping than the vertical wall.

The experiments show that the first wave to impact the coastal defence causes considerably more overtopping than subsequent waves. This is because coastal defences reflect wave energy which causes approaching waves to break. The approaching waves therefore have less energy so overtopping is reduced.

Investigation into key variables in the SPH code finds that an initial particle spacing of 2mm combined with a speed of sound of 20.12m/s and a value of δ -SPH of 0.1 is suitable for the model presented. This combination of parameters produces reasonable particle independence within the time frame considered, accurately predicts wave breaking and has a relatively constant pressure and density, showing almost incompressible behaviour of the fluid. Varying the speed of sound in the simulations causes unexpected fluctuations in density and pressure. Further investigation should be conducted into the effect of c_0 on the compressibility of the fluid.

The SPH models are shown to accurately predict free surface profiles for all coastal defences. As time increases the SPH predictions of free surface level diverge slightly from the experimental results. However, reasonable agreement is still up to the maximum time of the simulations at 15 periods.

Small, low energy waves caused by reflection are not accurately modelled by the SPH simulations, likely due to numerical diffusion in the code. Coastal defences which dissipate energy reduce these waves so in these cases the models represent the experiments more accurately.

Although the SPH simulations accurately predict the free surface profiles in the wave tank, overtopping is dramatically underestimated. Overtopping in the experimentation mostly occurs as green water, however in the simulations the overtopping is only caused by spray. This may be due to a combination of reasons, including numerical diffusion reducing wave energy, incorrect specification of viscosity or an insufficient number of particles to accurately predict fluid motion.

Further investigation into the affects of viscosity, numerical diffusion and particle number is required to improve the prediction of overtopping in the SPH model. This should be combined with investigation of a larger range of coastal defence configurations and wave conditions. This would enable the formulation of a comprehensive approach to predicting free surface profiles and wave overtopping using SPH.

References

- Corrado Altomare, AJC Crespo, BD Rogers, JM Domínguez, X Gironella, and M Gómez-Gesteira. Numerical modelling of armour block sea breakwater with smoothed particle hydrodynamics. *Computers & Structures*, 130:34–45, 2014.
- A Barreiro, AJC Crespo, JM Domínguez, and M Gómez-Gesteira. Smoothed particle hydrodynamics for coastal engineering problems. *Computers & Structures*, 120:96–106, 2013.
- George Keith Batchelor. *An introduction to fluid dynamics*. Cambridge university press, 2000.
- William Booker. *MSc Thesis: Experimental and Numerical Modelling of Coastal Processes*. University of Leeds, United Kingdom, 2015.
- Channel Coastal Observatory. *Regional Coastal Monitoring Programmes*. http://www.channelcoast.org/data_management/real_time_data/charts/ Accessed 15/06/2015, 2015.
- EM Coeveld, MRA Van Gent, and B Pozueta. Neural network: Manual nn_overtopping 2. *CLASH WP8, WL-Delft Hydraulics, Delft, The Netherlands*, 2005.
- AJC Crespo, JM Domínguez, BD Rogers, M Gómez-Gesteira, S Longshaw, R Canelas, R Vacondio, A Barreiro, and O García-Feal. Dualsphysics: Open-source parallel cfd solver based on smoothed particle hydrodynamics (sph). *Computer Physics Communications*, 187:204–216, 2015.
- Alejandro Jacobo Cabrera Crespo. Application of the smoothed particle hydrodynamics model sphysics to free surface hydrodynamics. *Universidade de Vigo*, 2008.
- Michael Dumbser. A simple two-phase method for the simulation of complex free surface flows. *Computer Methods in Applied Mechanics and Engineering*, 200(9):1204–1219, 2011.
- EurOtop Manual. Wave overtopping of sea defences and related structures-assessment manual. *UK: NWH Allsop, T. Pullen, T. Bruce. NL: JW van der Meer. DE: H. Schüttrumpf, A. Kortenhaus. www. overtopping-manual. com*, 2007.
- Robert A Gingold and Joseph J Monaghan. Smoothed particle hydrodynamics: theory and application to non-spherical stars. *Monthly notices of the royal astronomical society*, 181(3):375–389, 1977.
- M Gómez-Gesteira and Robert A Dalrymple. Using a three-dimensional smoothed particle hydrodynamics method for wave impact on a tall structure. *Journal of waterway, port, coastal, and ocean engineering*, 130(2):63–69, 2004.
- Thomas Goodfellow. *MSc Thesis: Experimental and Numerical Modelling of Coastal Processes*. University of Leeds, United Kingdom, 2015.

Steven A Hughes. *Physical models and laboratory techniques in coastal engineering*, volume 7. World Scientific, 1993.

JBA Consulting. *Homepage*. Jbaconsulting.com Accessed 15/06/2015, 2015.

Gerbrand J Komen, Luigi Cavaleri, Mark Donelan, Klaus Hasselmann, S Hasselmann, and PAEM Janssen. *Dynamics and modelling of ocean waves*. Cambridge university press, 1996.

Joe J Monaghan. Simulating free surface flows with sph. *Journal of computational physics*, 110(2):399–406, 1994.

A Panizzo, T Capone, and RA Dalrymple. Accuracy of kernel derivatives and numerical schemes in sph. *Submitted to Journal of Computational Physics*, 2007.

Richard S Thomas and Brian Hall. *Seawall design*. Butterworth-Heinemann, 1992.

Marcel RA van Gent, Henk FP van den Boogaard, Beatriz Pozueta, and Josep R Medina. Neural network modelling of wave overtopping at coastal structures. *Coastal Engineering*, 54(8):586–593, 2007.

A SPH Implementation

Chapter 5 describes several factors that affect the SPH formulation. In order to ensure the accuracy of simulations, investigation into the effect of these parameters are conducted. These investigations are summarised in section 6 and discussed in more detail here. Details and findings of the simulations used in this investigation are detailed in table 5.

Table 5: SPH Implementation Study Cases

Case N°	Particle Spacing d_p (mm)	N° of Particles	Aim	Description		Findings	
A1	1	105000	Particle Independence	Rotary Wave maker $T = 1\text{ s}$ $H = 20\text{ mm}$ $C_0 = 8.20 \text{ m/s}$		A2 and A3 show very good agreement up to 10T and good agreement at 20T. Observable change in volume caused by compressibility issues.	
A2	2	26250					
A3	5	4200					
A4	2	26250	Sound Speed Sensitivity Analysis	Tank with no wave maker	$C_0 = 8.20 \text{ m/s}$	Cases A4 and A6 produce significant variations in the free surface level, density and pressure. Case A5 shows only a small variation in these values.	
A5	2	26250			$C_0 = 20.50 \text{ m/s}$		
A6	2	26250			$C_0 = 32.81 \text{ m/s}$		
A7	2	26250		Wave maker	$C_0 = 8.20 \text{ m/s}$		
A8	2	26250	Sound Speed Sensitivity Analysis		$C_0 = 20.50 \text{ m/s}$	Cases A8 and A9 produce a sloped free surface at rest. Case A7 does not produce a sloped free surface but has a significant change in free surface level.	
A9	2	26250			$H = 20\text{ mm}$		
					$C_0 = 32.81 \text{ m/s}$		
A10	1	105000	Numerical Diffusion Analysis	Unforced Test $\text{Case } \delta\text{-SPH} = 0.1$ $C_0 = 20.50 \text{ m/s}$		Numerical diffusion damps out waves by 6 periods for all cases.	
A11	2	26250					
A12	5	4200					
A13	1	105000	Numerical Diffusion Analysis	Forced Test Case $\delta\text{-SPH} = 0.1$ $C_0 = 20.50 \text{ m/s}$		In each case waves are damped to approximately 50% of their original height across the domain	
A14	2	26250					
A15	5	4200					
A16	2	26250	Numerical Diffusion Analysis	Unforced Test Case	$\delta\text{-SPH} = 1.0$	Increasing $\delta\text{-SPH}$ slightly reduces damping rate but causes an increase in fluid volume	
A17	2	26250			$\delta\text{-SPH} = 0.5$		
A18	2	26250			$\delta\text{-SPH} = 0.1$		
A19	2	26250	Numerical Diffusion Analysis	Forced Test case	$\delta\text{-SPH} = 1.0$		
A20	2	26250			$\delta\text{-SPH} = 0.5$		
A21	2	26250			$\delta\text{-SPH} = 0.1$		
A22	1	105000	Particle Independence	Rotary Wave maker $T = 1\text{ s}$ $H = 20\text{ mm}$ $C_0 = 20.50 \text{ m/s}$ $\delta\text{-SPH} = 1.0$		Cases A22 and A23 show good agreement at 10T and reasonable agreement at 20T.	
A23	2	26250					
A24	5	4200					

A.1 Initial Particle Independence Study

An initial particle independence study is conducted to assess the affect that particle spacing has on the simulations and determine an appropriate initial particle spacing to use. The wave tank (figure 4) is modelled with a rotary paddle wave maker using values of d_p of 1mm (Case A1), 2mm (Case A2) and 5mm (Case A3).

After ten periods all three cases remain in phase with one another (figure A.1). By 20T (figure A.2) case A3 is slightly out of phase with cases A1 and A2 which are in phase with one another.

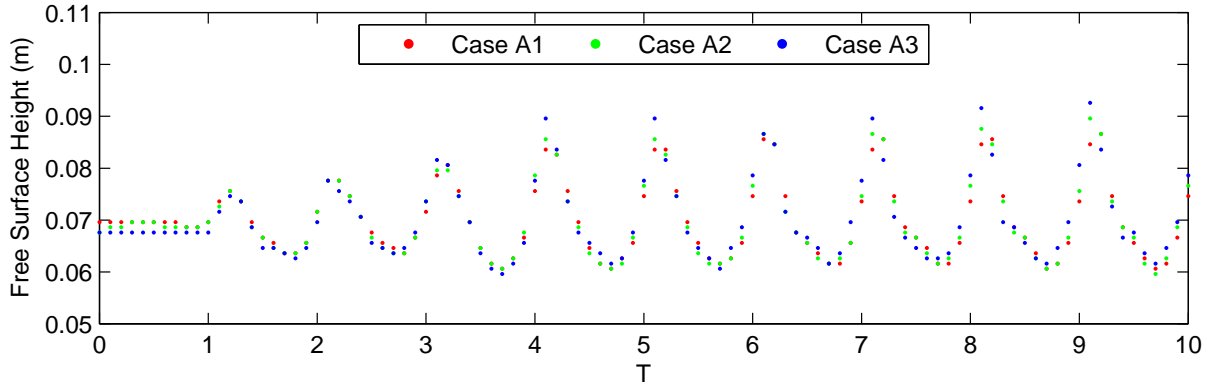


Figure A.1: Free Surface Height at $x=0.75\text{m}$. Case A1: $d_p = 1\text{mm}$. Case A2: $d_p = 2\text{mm}$. Case A3 $d_p = 5\text{mm}$

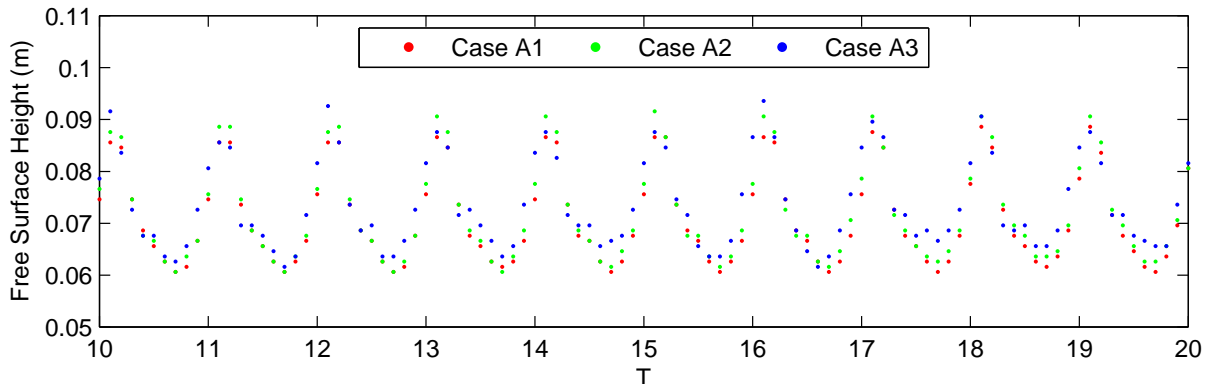


Figure A.2: Free Surface Height at $x=0.75\text{m}$. Case A1: $d_p = 1\text{mm}$. Case A2: $d_p = 2\text{mm}$. Case A3 $d_p = 5\text{mm}$

After five periods the free surface profiles of the three cases are very similar, with case A3 showing slightly less agreement than the other two cases.

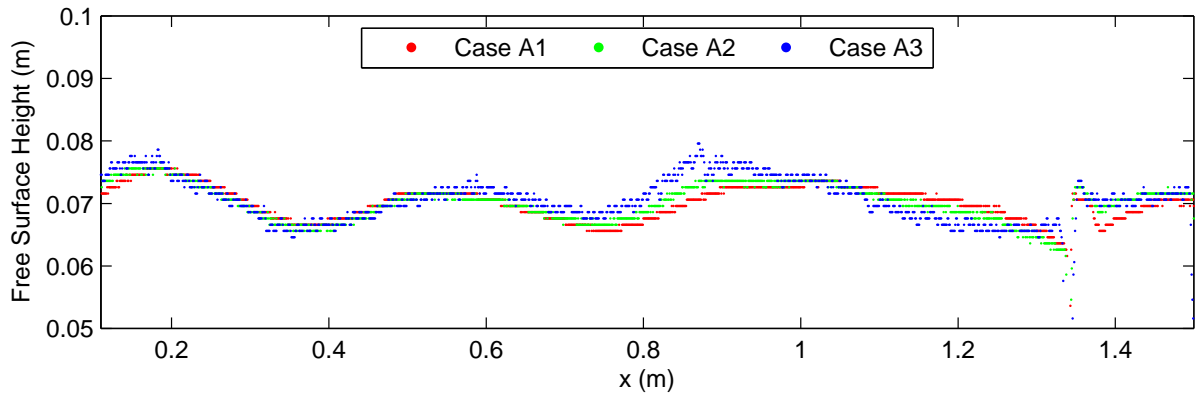


Figure A.3: Free Surface Profiles at 5T. Case A1: $dp = 1\text{mm}$. Case A2: $dp = 2\text{mm}$. Case A3 $dp = 5\text{mm}$

At 10T a similar free surface profile is shown by all three cases (figure A.4). However in case A3 there are small localised fluctuations in the free surface elevation and a noticeable height difference in some positions. Cases A1 and A2 show close agreement, with a maximum free surface height difference of 2mm.

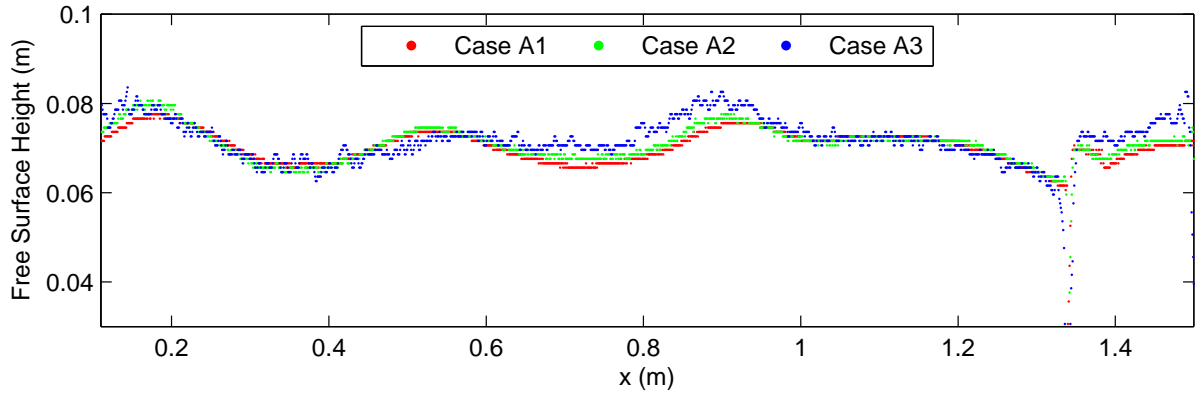


Figure A.4: Free Surface Profiles at 10T. Case A1: $dp = 1\text{mm}$. Case A2: $dp = 2\text{mm}$. Case A3 $dp = 5\text{mm}$

Figure A.5 shows that at 20T the free surface profiles of cases A1 and A2 are reasonably close, with a maximum height difference of 3mm. Case A3 shows large differences in free surface height significant localised fluctuations.

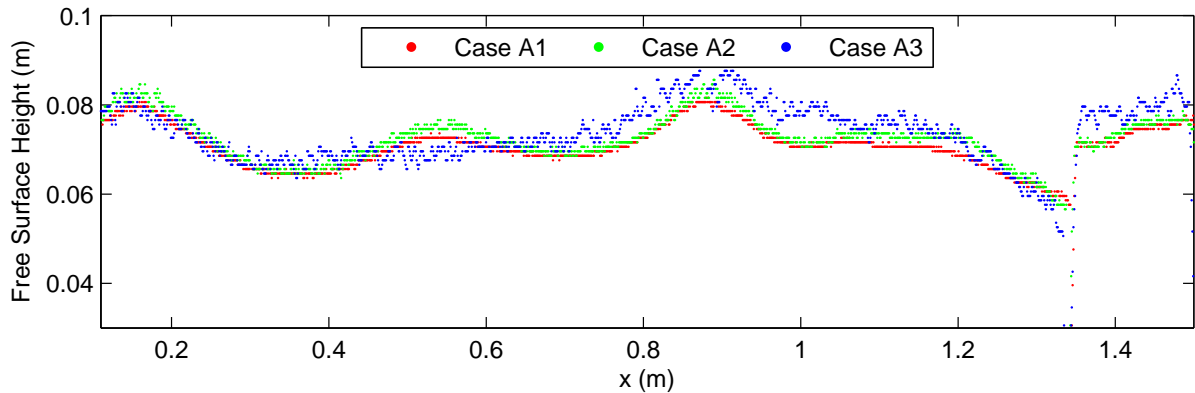


Figure A.5: Free Surface Profiles at 20T. Case A1: $dp = 1\text{mm}$. Case A2: $dp = 2\text{mm}$. Case A3 $dp = 5\text{mm}$

Figure A.6 shows the free surface profiles at 0T and figure A.7 shows the free surface profiles at 60T where the wavemaker has been stopped and the fluid allowed to come to rest for 20 periods. The fall in free surface height at $x = 1.36\text{m}$ is due to the position of the wave maker. It can be seen that once the fluid has come to rest there is a significant change in the resting free surface level, showing an increase in the fluid volume.

Note that the three cases do not have the same initial free surface level at 0T. This is due to the method by which the DualSPHysics code calculates the position of the free surface. At the free surface there is a distinct change in mass. The mass of each particle is used as a reference mass. At each particle the mass is interpolated using the surrounding particles and if the mass falls below 40% of the reference mass (for 2D simulations) the z position is recorded as the free surface level. Larger particle spacing results in this threshold value occurring at a lower z position due to the lower position of the centroid of the topmost particle.

This particle independence study shows that cases A1 and A2 produce very similar results after 10 periods and good agreement after 20 periods. The study also shows that the volume of fluid in the simulations changes by up to 8.9%. This phenomenon is discussed further in section A.2

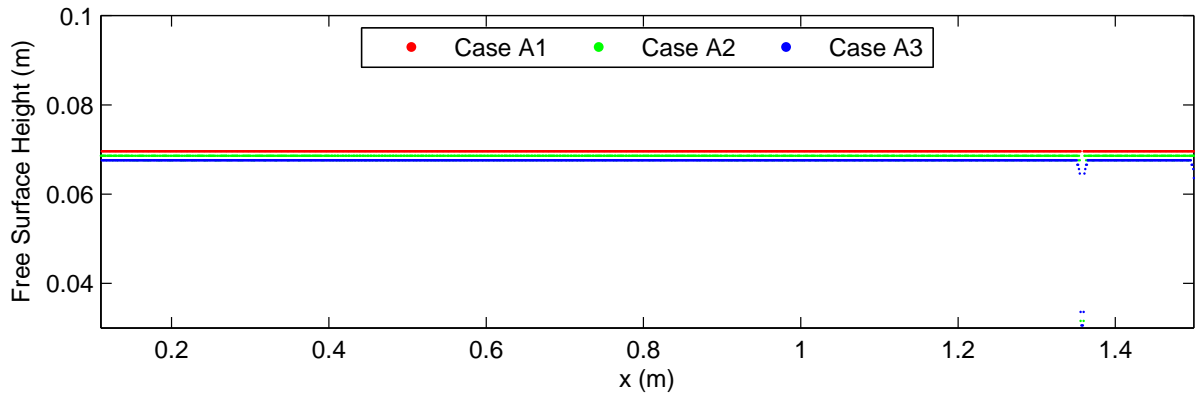


Figure A.6: Free Surface Profiles at 0T. Case A1: $dp = 1\text{mm}$. Case A2: $dp = 2\text{mm}$. Case A3 $dp = 5\text{mm}$

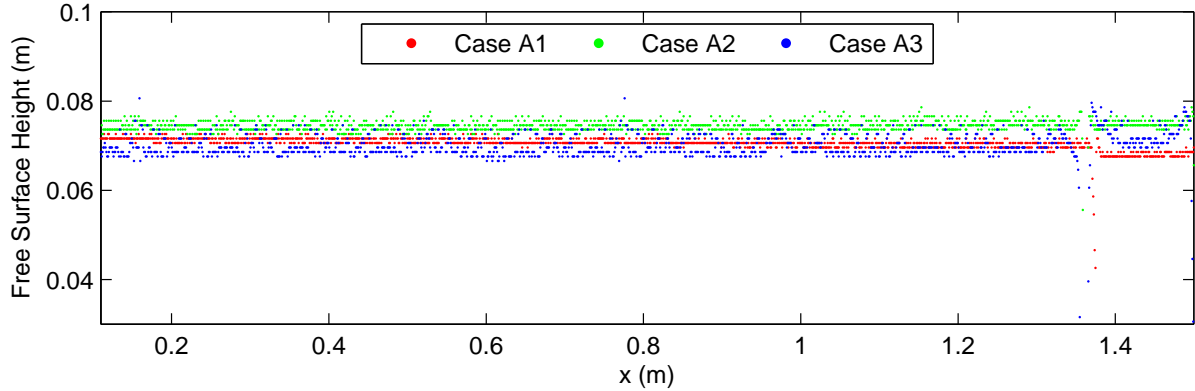


Figure A.7: Free Surface Profiles at 60T. Case A1: $dp = 1\text{mm}$. Case A2: $dp = 2\text{mm}$. Case A3 $dp = 5\text{mm}$

A.2 Sound Speed Sensitivity Analysis

The particle independence study discussed in section A.1 finds that the volume of fluid in the simulations changes, showing compressible behaviour of the fluid. The DualSPHysics code treats the fluid as weakly compressible and relates the speed of sound in the simulation to density and pressure with equations 16 and 18.

Cases A1, A2 and A3 have a speed of sound of 8.05 m/s with maximum fluid velocity of 0.7 m/s. According to Monaghan (1994) this value of C_0 should not affect the fluid as it is greater than ten times the maximum fluid speed, however, this is not the case. Sensitivity analysis is conducted in order to determine an appropriate speed of sound to produce a constant fluid volume in the wave tank with an acceptable computational cost.

In the DualSPHysics code the speed of sound is calculated by:

$$c_0 = coef_{sound} \sqrt{g \cdot h_{swl}} \quad (22)$$

where $coef_{sound}$ is a parameter which can be chosen and h_{swl} is the depth of the fluid at rest. It is advised that the value of $coef_{sound}$ should not be greater than 40, however this is possible if required.

Simulations are conducted in a 1.5m long rectangular tank with no wave maker to assess the volume change with no energy input. Sufficient time is allowed for each simulation to come to rest.

From figure A.2 it can be seen that in all three cases there is a change in volume and also that in cases A4 and A5 the free surface is sloped. It is unclear why this is. Table A.2 shows that as c_0 increases the change in volume reduces, eventually becoming negative. The smallest change in volume occurs at $coef_{sound} = 25$. Increasing c_0 also increases the slope of the free surface.

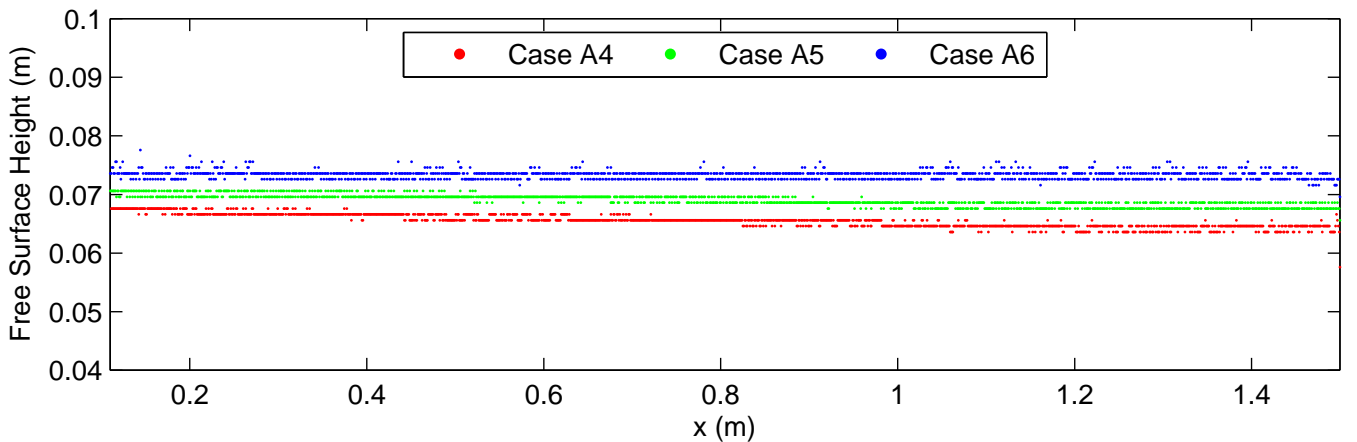


Figure A.8: Free Surface Profiles at 35s. Case A4: $c_0 = 32.19\text{m/s}$. Case A5 $c_0 = 20.12\text{m/s}$. Case A6: $c_0 = 8.05\text{m/s}$

Table 6: Volume Change and Free Surface Angle for Varying Values of c_0 at t=35s

Case N°	$coef_{sound}$	c_0 (m/s)	% Change in Volume	Free Surface Slope (°)
A4	40	32.19	-3.28×10^{-2}	0.172
A5	25	20.12	7.29×10^{-3}	0.076
A6	10	8.05	6.56×10^{-2}	0

Pressure and Density Variations

Equation 16 is used to derive an expression for the pressure within the fluid:

$$p = B \left[\left(1 + \frac{p}{B}\right)^{\frac{\gamma-1}{\gamma}} - \left(\frac{\gamma-1}{\gamma}\right) \cdot \frac{\rho_0 g z}{B} \right]^{\frac{\gamma}{\gamma-1}} - B. \quad (23)$$

(Goodfellow, 2015)

The density of the fluid is then calculated by

$$\rho = \rho_0 \left(1 + \frac{p}{B}\right)^{\gamma-1}. \quad (24)$$

These results are then compared to the recorded values of the SPH simulations.

Figures A.2 and A.2 show the pressure and density calculated by the analytical solution and the values recorded by the SPH simulations. Both the pressure and density increase over time with a lower value of c_0 and decrease with a higher speed of sound. At $c_0 = 20.12$ m/s the pressure and density remain relatively constant as is to be expected as this value of c_0 produced a minimal change in the free surface level. This is counter intuitive as an expanding fluid with the same number of particles would be expected to reduce in density and a contracting fluid would be expected to increase in density. However this is due to the manner by which the DualSPHysics code measures the height of the free surface.

At the free surface there is a sudden change in mass. The mass of a point, b , at some value of z far above the free surface is calculated from the mass of the neighbouring particles by

$$m_b = \sum_a m_a \left(\frac{W_{ab} m_a}{\rho_a} \right). \quad (25)$$

(Crespo, 2008)

The mass is calculated for a specified number of positions below the initial measurement. The position of the free surface is recorded where the value of m_b becomes larger than a reference mass m_{ref} .

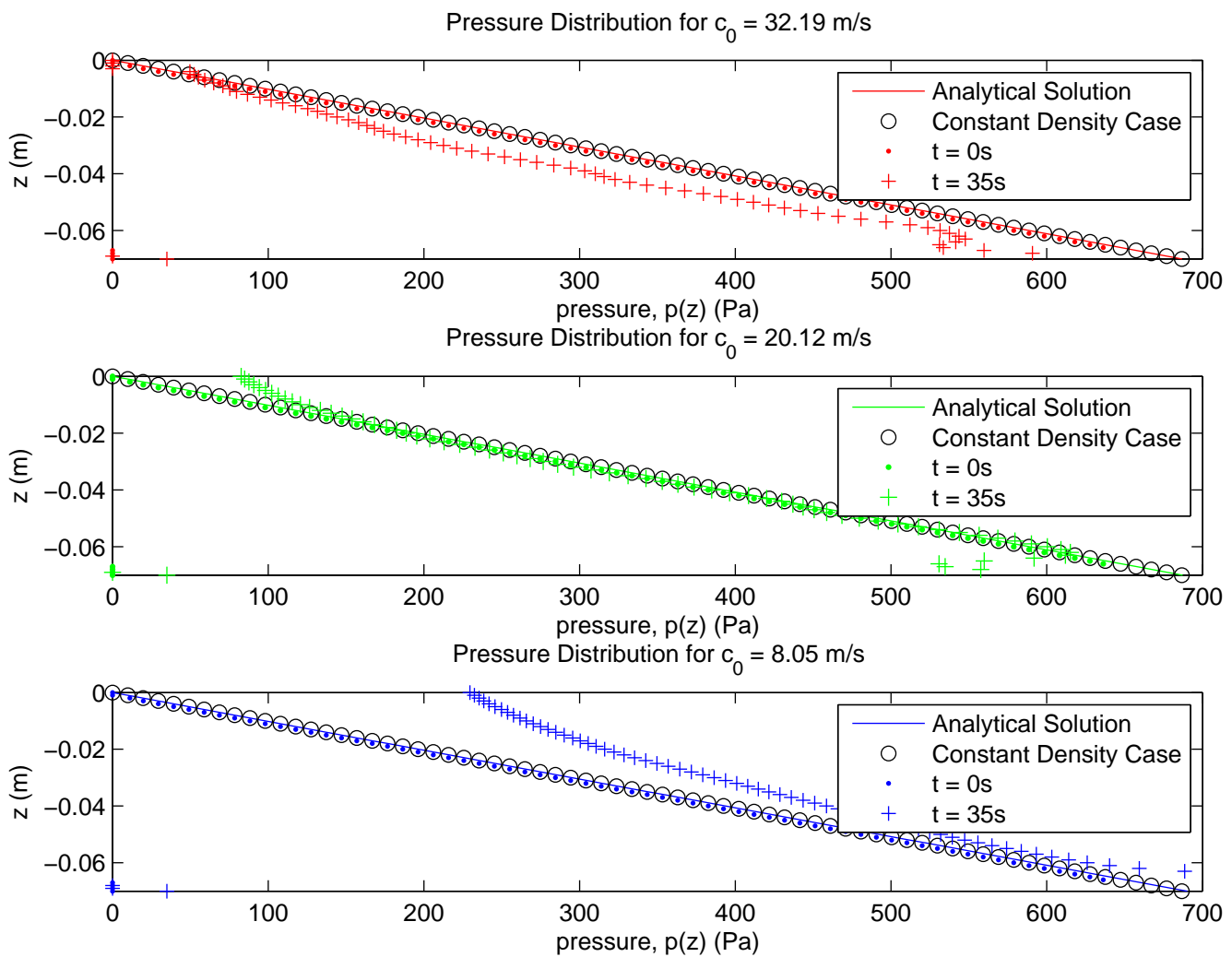


Figure A.9: Changes in Pressure for Varying Values of c_0

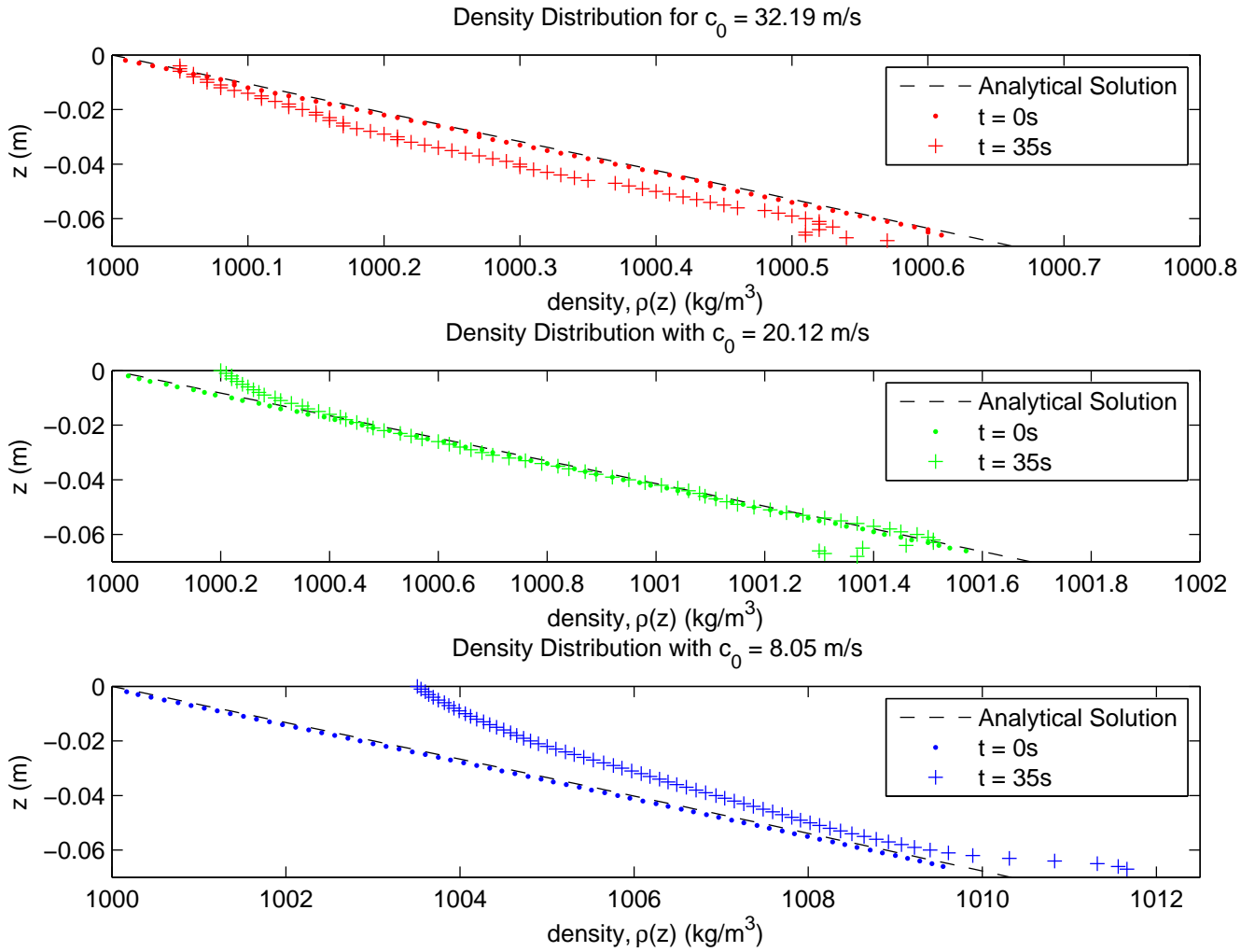


Figure A.10: Changes in Density for Varying Values of c_0

Figure A.11 shows the mass values of the three cases at $x=0.75\text{m}$. In case A6, where the level of the free surface increases, the mass above the initial free surface level must also increase. If the density were to reduce, as would be expected for an expanding fluid, then the interpolated mass at the free surface would also reduce so the value of the free surface would be recorded as lower than its initial position. Similarly, in case A4 where the free surface level decreases, an increase in density would increase the interpolated mass at higher values of z so the free surface would be measured at a higher position. Therefore, if the total mass of the fluid increases, and the number of fluid particles remains the same, the density must also increase.

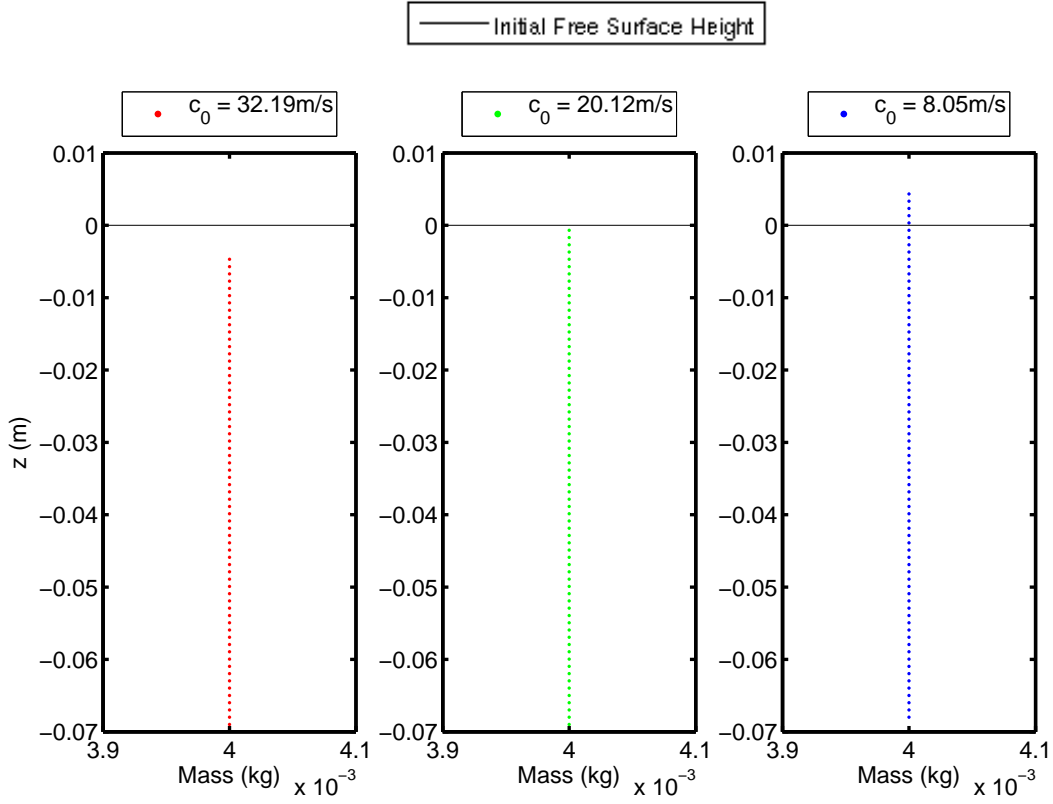


Figure A.11: Fluid Mass for Varying Values of c_0 at $t=35s$

This, however, does not explain why the pressure and density values derived from equation 16 do not match the values produced in the simulations. It is possible that there are other factors influencing the results other than those discussed in section 5.

Simulations are also conducted in the same tank with a rotary wave maker. The wave period is one second and the wave height is 20mm. The wave maker runs for 40s and the simulation continues for a further 20s to allow the fluid to come to rest. Figure A.12 shows that in all cases there was again a noticeable change in volume. In cases 4.5 and 4.6 there is a significant difference in the level of the free surface on either side of the wave maker and again a sloped free surface between $x=0$ and the wave maker. Table 7 shows the percentage volume change and also the free surface slope between $x=0$ and the wave maker for the three cases. Again the smallest volume change occurs at $coef_{sound} = 25$ and the slope of the free surface increases as the speed of sound increases.

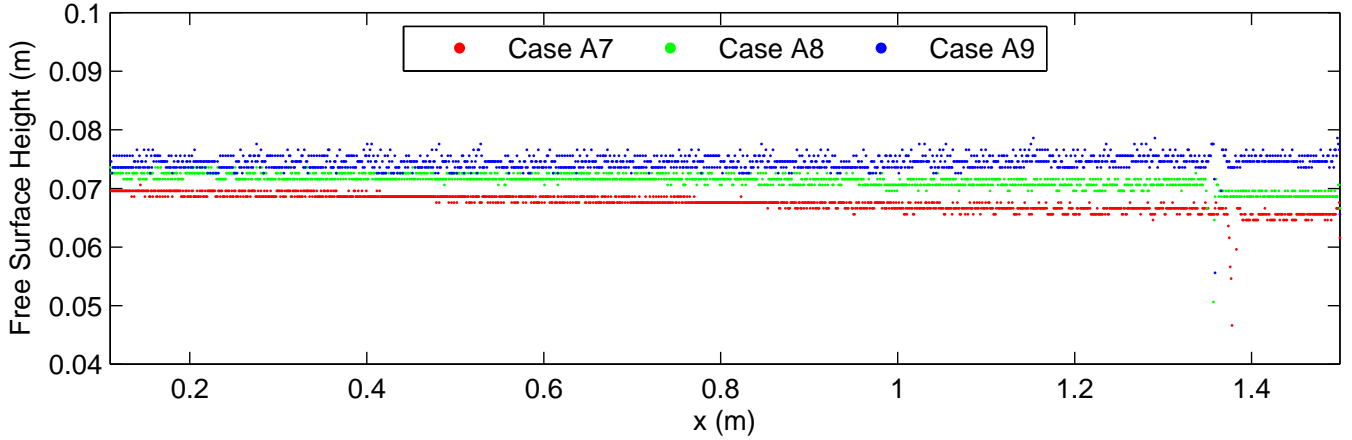


Figure A.12: Free Surface Profiles of Varying Values of c_0 at 60s

Table 7: Free Surface Profiles at 60s. Case A4: $c_0 = 32.19\text{m/s}$. Case A5 $c_0 = 20.12\text{m/s}$. Case A6: $c_0 = 8.05\text{m/s}$

Case N°	$coef_{sound}$	c_0 (m/s)	% Change in Volume	Free Surface Slope ($^{\circ}$)
A7	40	32.19	-8.76×10^{-2}	0.167
A8	25	20.12	3.89×10^{-2}	0.003
A9	10	8.05	8.81×10^{-2}	0

The results of the sound speed sensitivity analysis show that $c_0 = 20.12\text{m/s}$ produces the smallest change in volume, pressure and density. At this speed there is a relatively small slope to the free surface but it is considered preferable to the larger volume change produced with a lower speed of sound. The computational time of this speed of sound is also considerably less than for $c_0 = 32.19\text{ m/s}$.

A.3 Test Cases

A.3.1 Unforced Case

Section 6.3 describes the unforced test case that is implemented in DualSPHysics using three values of dp , 1mm (Case A10), 2mm (Case A11) and 5mm (Case A12). The three cases have the same starting position as the unforced analytical solution (figure A.13). Note that angular profile of the initial free surfaces is due to the coarseness of the initial particle positions.

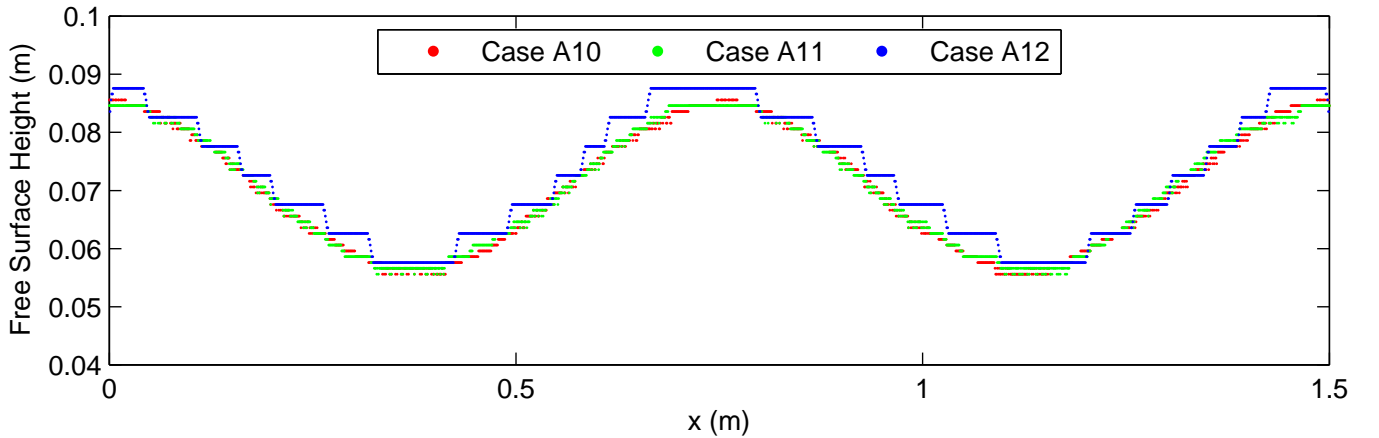


Figure A.13: Unforced Test Case at $t=0s$. Case A10: $dp = 1mm$. Case A11: $dp = 2mm$. Case A12 $dp = 5mm$

Figure A.14 shows the potential energy of the three SPH cases and the unforced test case. The potential energy of the test case remains constant as no viscous forces are accounted for. The three SPH cases damp due to numerical diffusion at roughly the same rate, reaching their minimum energy after around 6 periods. Note that the cases have different energy values at $0T$. This is due to the resolution of the initial particle spacing causing the larger values of dp to have a higher initial free surface level. Taking this initial energy difference into account the three cases diffuse at roughly the same rate to approximately the same energy after six periods.

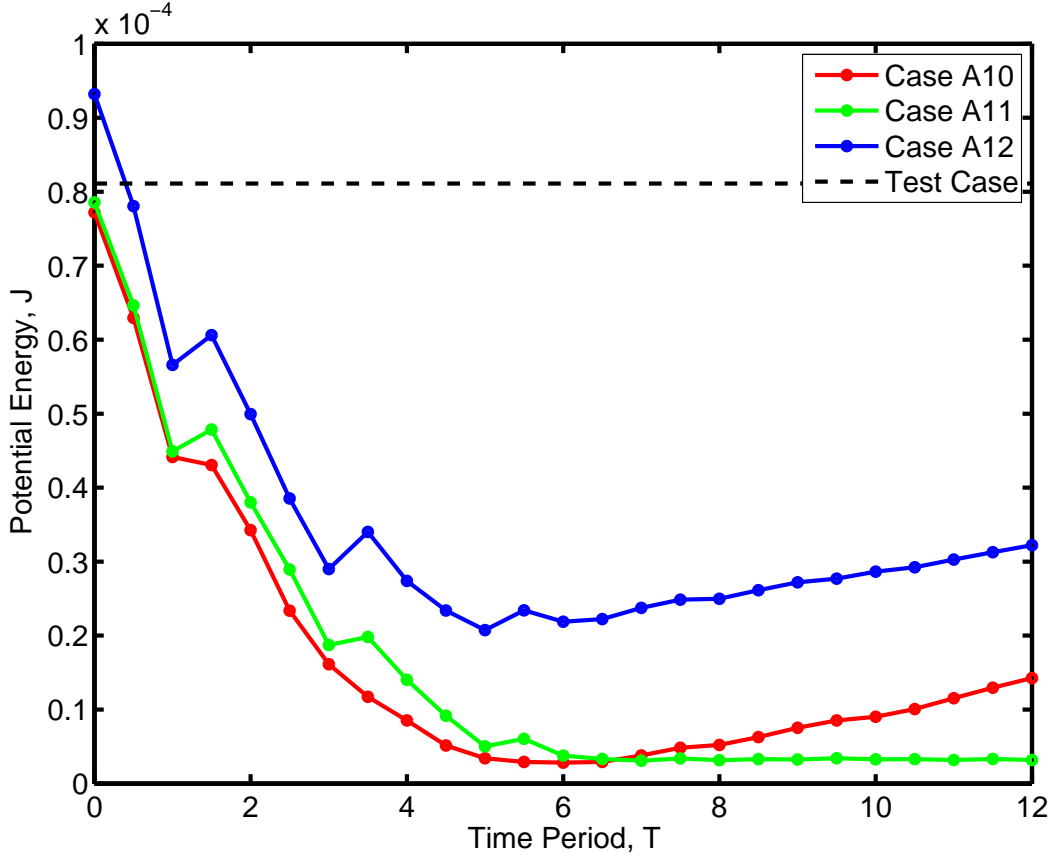


Figure A.14: Potential Energy of Unforced Standing Wave. Case A10: $dp = 1\text{mm}$. Case A11: $dp = 2\text{mm}$. Case A12 $dp = 5\text{mm}$

Figure A.14 also shows that after $6T$ the potential energy of cases A10 and A12 begins to increase. This is due to the compressibility issues discussed in Appendix A.2. causing an increase in the fluid volume demonstrating that the compressibility of the fluid is affected by particle spacing as well as the speed of sound. Case A11 shows relatively constant potential energy which is to be expected as the parameters of this case are the same as those of case A4 where a minimal volume change was observed.

A.3.2 Forced Case

The forced case was simulated with a wave number, $k = 9$ for three different particle spacings 1mm (Case A13), 2mm (Case A14) and 5mm (Case A15). In all three cases the piston wave maker produces waves with the same amplitude as the test case. In the simulations the boundary moves horizontally by half the specified displacement from its initial starting position before beginning its regular piston motion. This creates a wave roughly half height of the test case which is reflected and interferes with approaching incident waves. This interference is combined with the changing domain length so that the three cases become completely out of phase with the forced test case after only 6 periods (figure A.15).

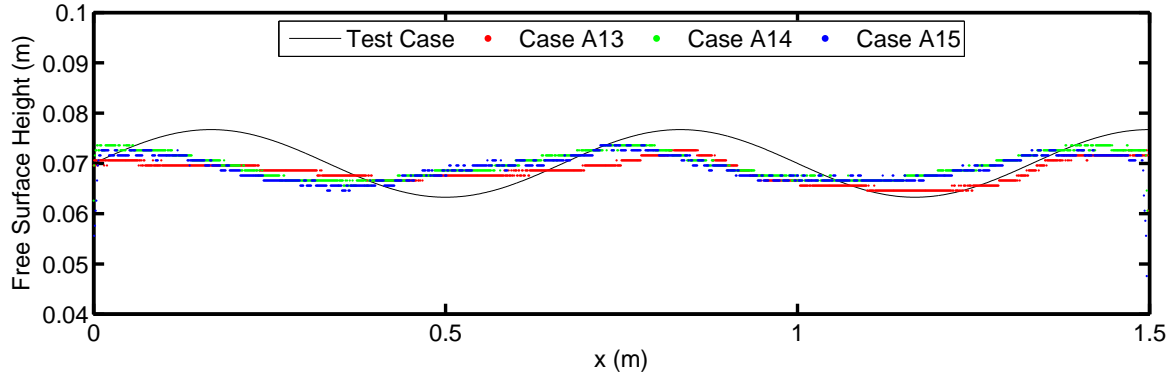


Figure A.15: Free Surface Profiles at 6T. Case A13: $dp = 1\text{mm}$. Case A14: $dp = 2\text{mm}$. Case A15 $dp = 5\text{mm}$

The interference caused by the first wave also means that the total damping of the wave as it propagates across the domain cannot be directly observed. The wave heights for each case are therefore compared to the forced test case at 1.5T, 2T and 2.5T before the initial wave is reflected (figure A.16). The total reduction in wave height across the length of the domain is then extrapolated from these results. Like the unforced test case the initial wave of the three cases damp out at approximately the same rate, with a total reduction in wave height of around 50% across the length of the tank.

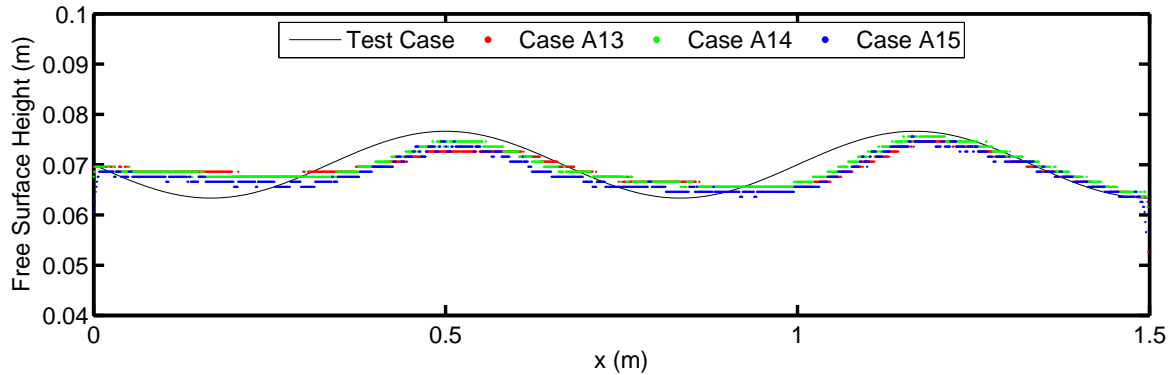


Figure A.16: Free Surface Profiles at 2.5T. Case A13: $dp = 1\text{mm}$. Case A14: $dp = 2\text{mm}$. Case A15 $dp = 5\text{mm}$

δ -SPH Analysis

The δ -SPH function is a parameter which controls numerical diffusion in the DualSPHysics formulation. The unforced and forced test cases are repeated with three values of δ -SPH and an initial particle spacing of 2mm to establish how the numerical damping is affected.

Unforced Case Figure A.17 shows the total potential energy of the fluid for three values of δ -SPH, 1.0 (Case A16), 0.5 (Case A17) and 0.1 (Case A18). As in the previous unforced test cases the energy is damped to its minimum value after around 6 periods. Each of the three cases have the same initial energy as a value of 2mm was used for each case. Increasing the value of δ -SPH slightly reduces the rate at which damping occurs. It can be seen from figure A.17 that the total energy of cases A16 and A17 begins to increase after it has reached its minimum value. This is due to the affect that δ -SPH has on density fluctuations in the fluid.

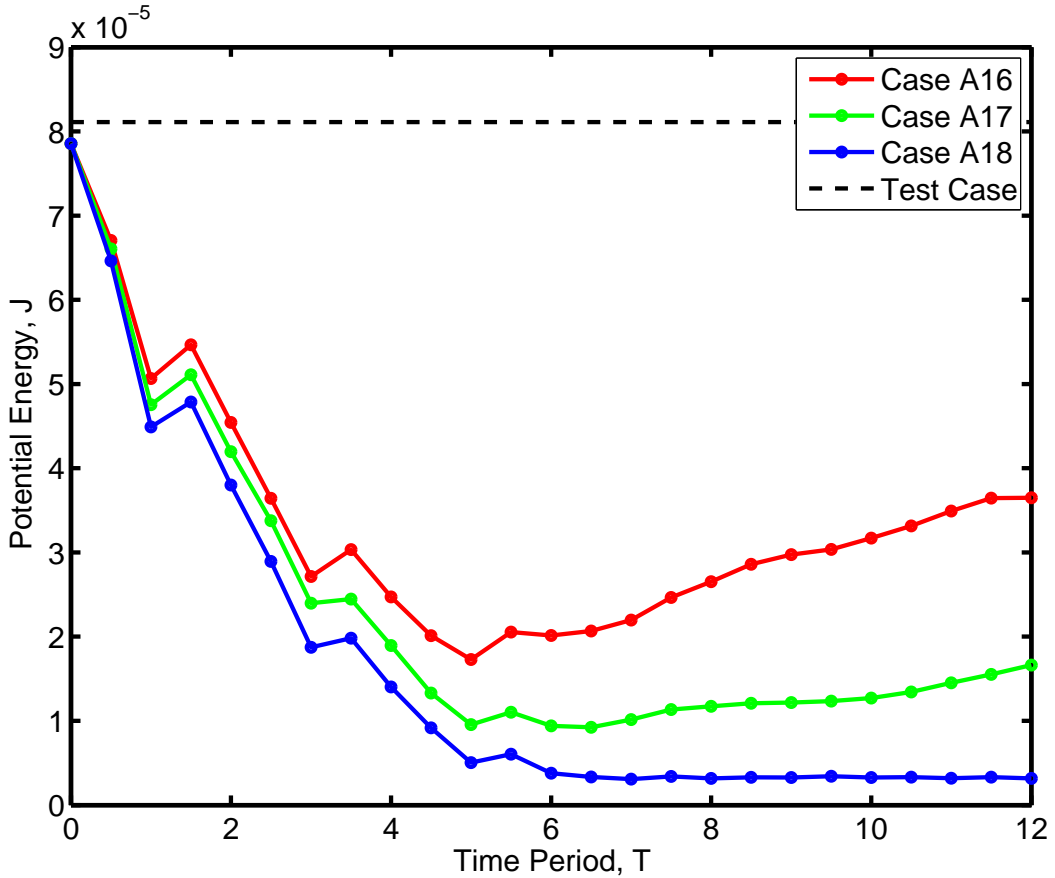


Figure A.17: Potential Energy of Unforced Standing Wave. Case A16: δ -SPH = 1.0. Case A17: δ -SPH = 0.5. Case A18 δ -SPH = 0.1

Forced Case The total damping over the domain is calculated in the same manner as the previous forced test cases. Again, a δ -SPH value of 0.1 produced a total damping of 50% across the length of the tank. Case A20 (δ -SPH = 0.5) produced a total damping of 63% and case A19 (δ -SPH = 1.0) produced a total damping of 70%.

δ -SPH Summary

Increasing the value of δ -SPH reduces the numerical diffusion in the system but causes issues with the compressibility of the fluid. Simulations utilising various values of δ -SPH are compared with experimental data to determine an appropriate value.

A.4 Revised Particle Independence Study

The previous particle independence study is repeated with the revised speed of sound of 20.12 m/s. Figure A.18 shows the free surface height at $x = 0.75\text{m}$ between $0T$ and $10 T$. After ten periods the three cases remain in phase with one another. At this time it can be seen that as the particle spacing increases the level of the free surface also increases. This can be seen more clearly in figures A.19 and A.20 where a difference in fluid volume between the three cases is observable. In Appendix A.2 a sound speed of 20.12m/s was found to produce a minimal change in volume with a particle spacing of 2mm. Cases A22 ($dp = 1\text{mm}$), A23 ($dp = 2\text{mm}$) and A24 ($dp = 5\text{mm}$) show that the compressibility of the fluid in the SPH simulation is dependent on the particle spacing as well the speed of sound. At $20T$ (figure A.19) the difference in free surface height is more pronounced but the three simulations remain relatively closely in phase.

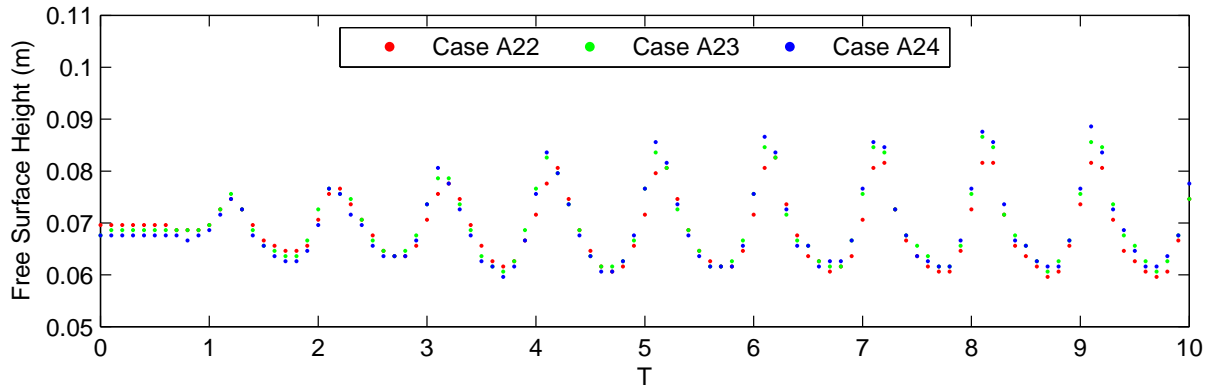


Figure A.18: Free Surface Height at $x=0.75$. Case A22: $dp = 1\text{mm}$. Case A23: $dp = 2\text{mm}$. Case A24 $dp = 5\text{mm}$

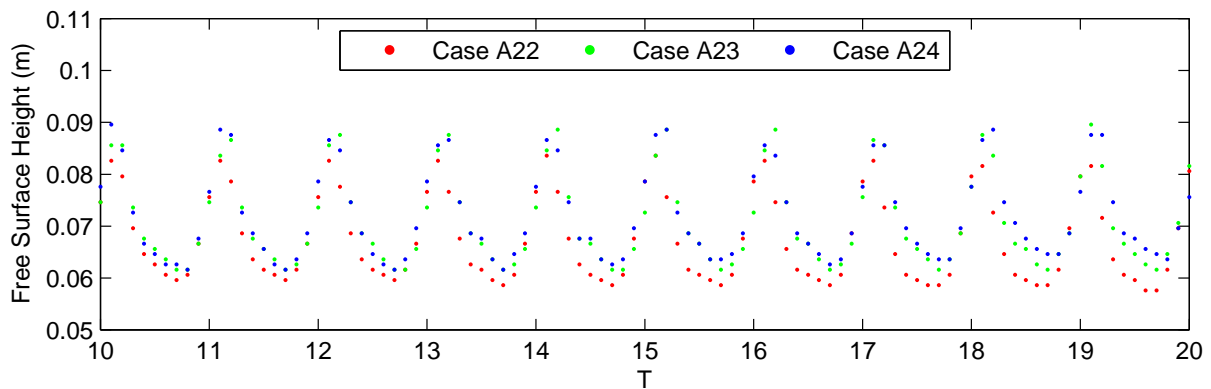


Figure A.19: Free Surface Height at $x=0.75$. Case A22: $dp = 1\text{mm}$. Case A23: $dp = 2\text{mm}$. Case A24 $dp = 5\text{mm}$

Figure A.20 shows the free surface profiles at $10T$. The differences in fluid volume can between the cases are seen, however the three cases show very good agreement on the wave profile at this

time.

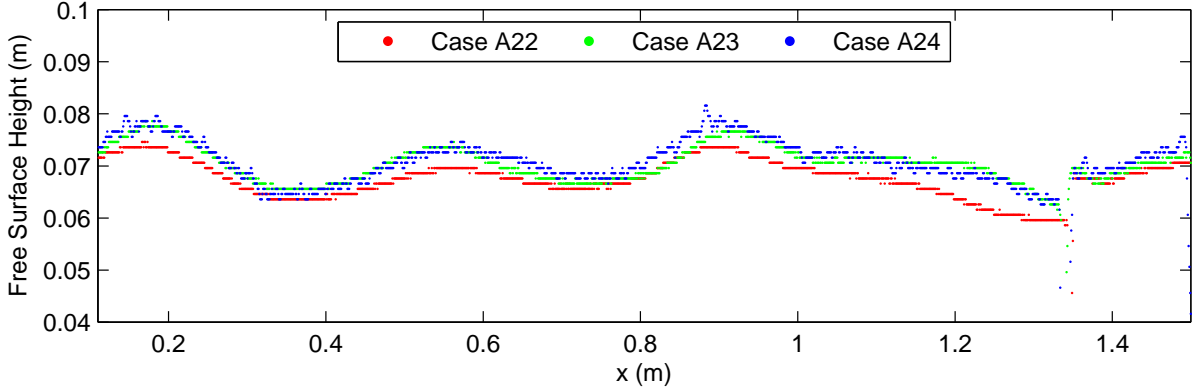


Figure A.20: Free Surface Profiles at 10T. Case A22: $d_p = 1\text{mm}$. Case A23: $d_p = 2\text{mm}$. Case A24 $d_p = 5\text{mm}$

At 20T (figure A.21) the differences in fluid volume are more pronounced. Cases A22 and A23 still show reasonable close agreement in the general profile of the free surface. The profile of case A24 shows less agreement and significant localised fluctuations in the free surface height are apparent.

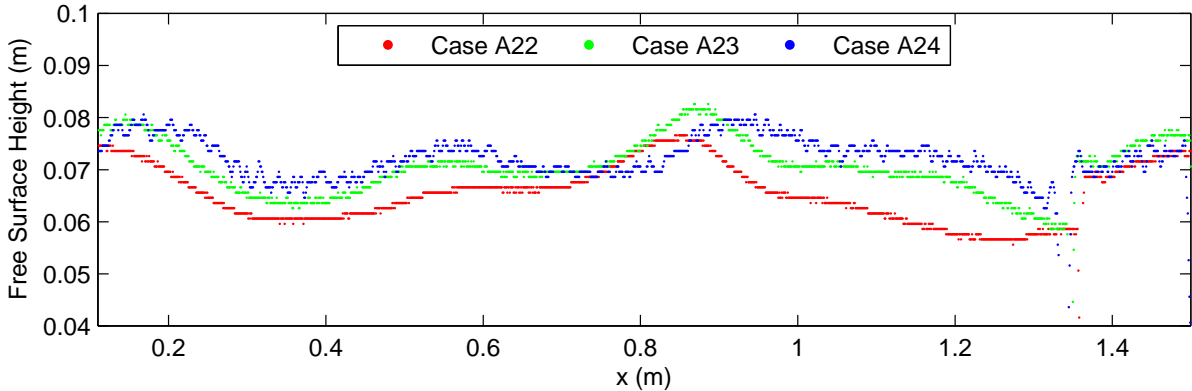


Figure A.21: Free Surface Profiles at 20T. Case A22: $d_p = 1\text{mm}$. Case A23: $d_p = 2\text{mm}$. Case A24 $d_p = 5\text{mm}$

Revised Particle Independence Summary

This study has shown that the compressibility of fluid in the SPH simulations is dependent on both the speed of sound and the particle spacing. With the changes in fluid volume taken into account cases A22 and A23 show reasonable agreement after 20 periods but show significant divergence at 25 periods and are unreliable by 30T.

A.5 Conclusions of SPH Implementation Studies

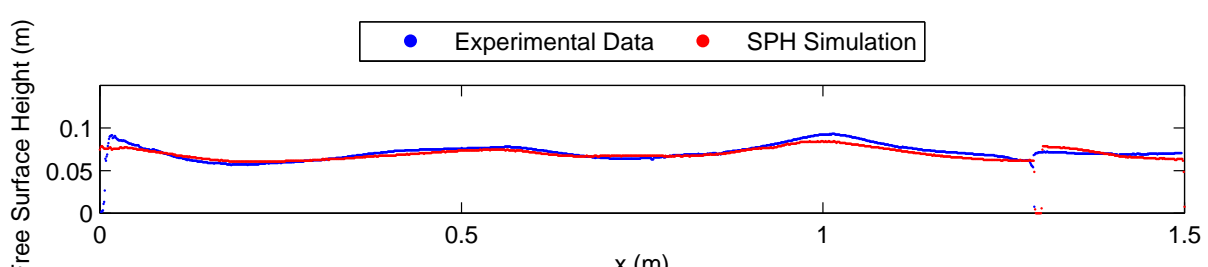
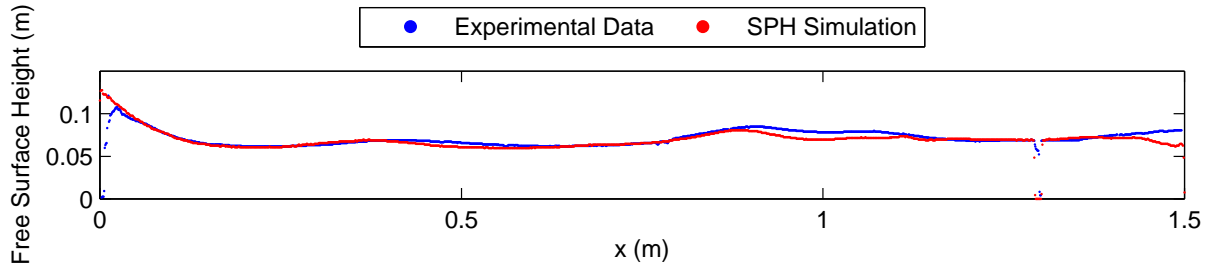
Several variables in the SPH formulation are investigated. From the results of this investigation it is decided that an initial particle spacing of 2mm combined with a sound speed of 20.12 m/s is appropriate for simulation of the wave tank. This combination of parameters provides reasonable particle independence and only small variations in fluid volume, pressure and density. Comparisons with experimental data are made in section 7 to determine an suitable value of δ -SPH.

B Further Results

The results of the experimentation and SPH simulations are discussed in detail in chapter 7. This Appendix contains further details of the results of this project.

B.1 Single Wave

B.1.1 Vertical Wall



B.1.2 1 in 2 Slope

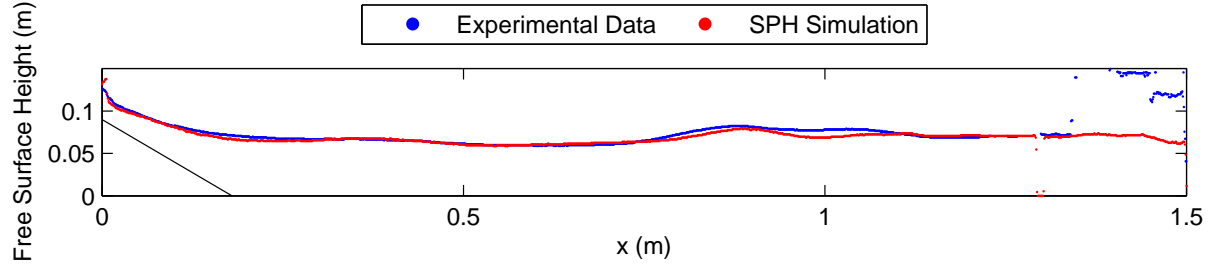


Figure A.24: Free Surface Profiles of Experimentation and SPH simulation at $t=2.7\text{s}$

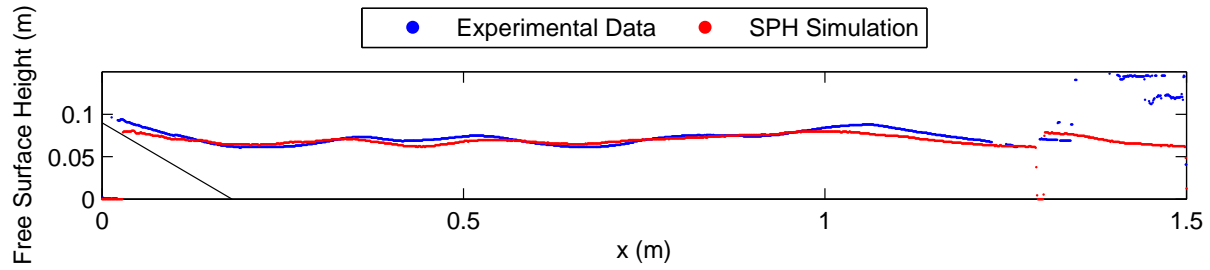


Figure A.25: Free Surface Profiles of Experimentation and SPH simulation at $t=4.0\text{s}$

B.1.3 1 in 3 Slope

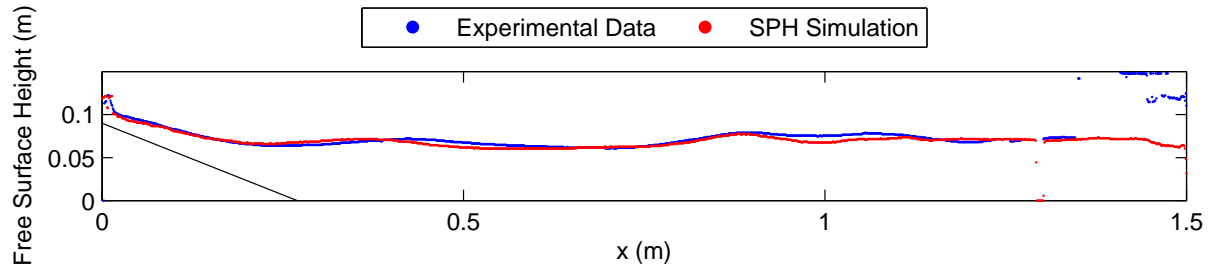


Figure A.26: Free Surface Profiles of Experimentation and SPH simulation at $t=2.7\text{s}$

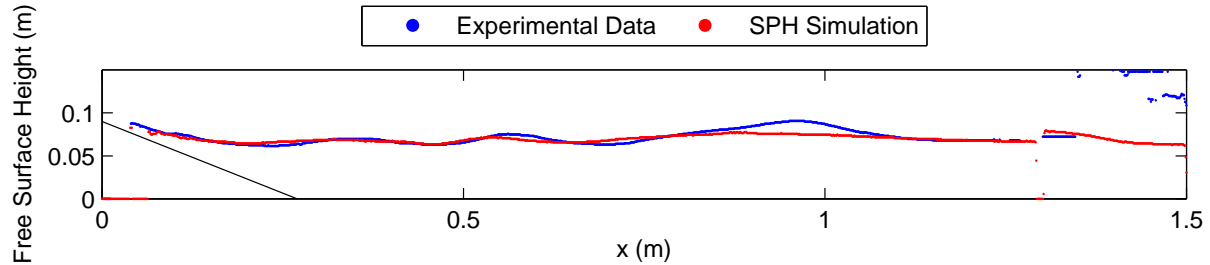


Figure A.27: Free Surface Profiles of Experimentation and SPH simulation at $t=4.0\text{s}$

B.1.4 Stepped Slope

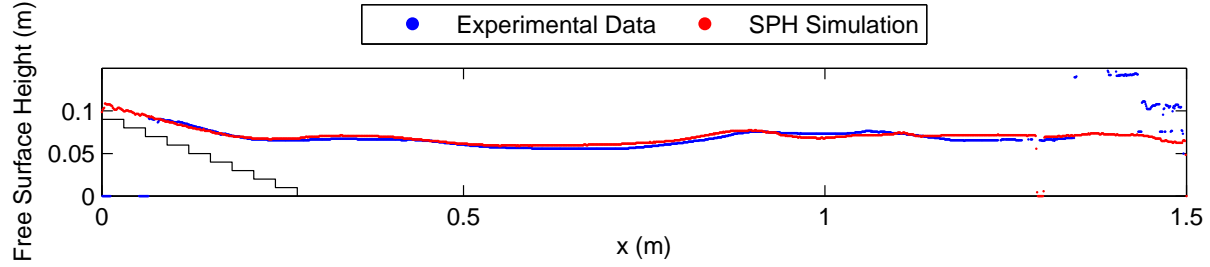


Figure A.28: Free Surface Profiles of Experimentation and SPH simulation at $t=2.7\text{s}$

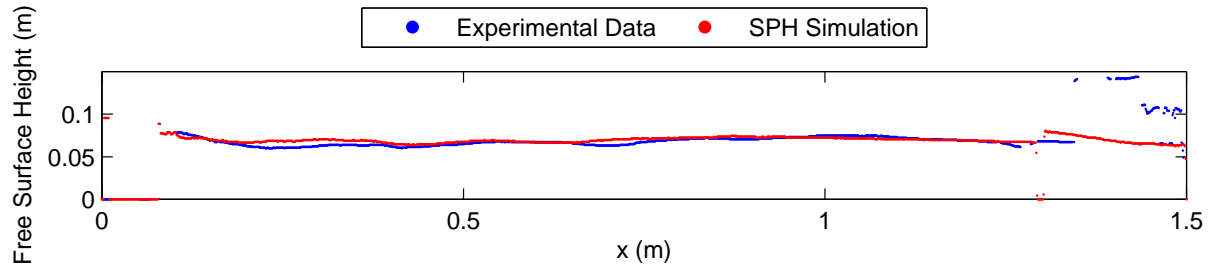


Figure A.29: Free Surface Profiles of Experimentation and SPH simulation at $t=4.0\text{s}$

B.1.5 Recurved Wall

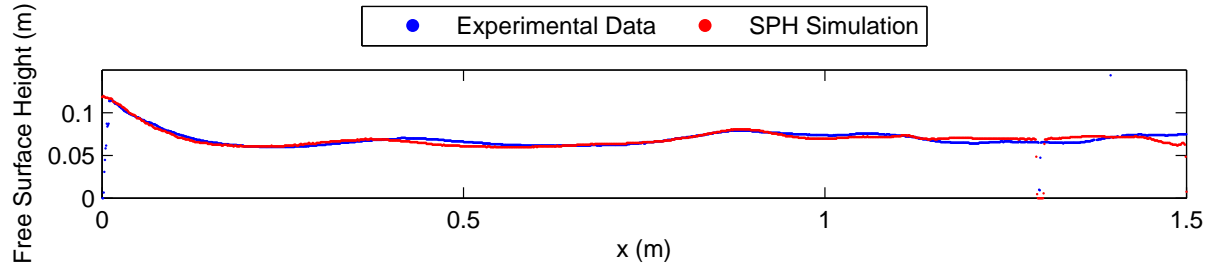


Figure A.30: Free Surface Profiles of Experimentation and SPH simulation at $t=2.7\text{s}$

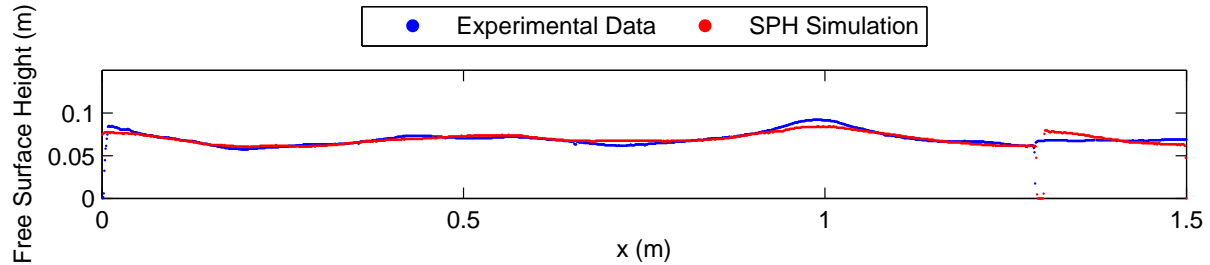


Figure A.31: Free Surface Profiles of Experimentation and SPH simulation at $t=4.0\text{s}$

B.2 Continuous Wave

B.2.1 Vertical Wall

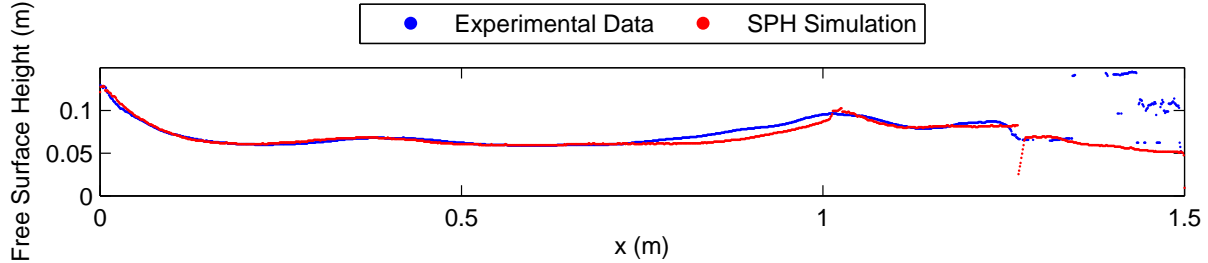


Figure A.32: Free Surface Profiles of Experimentation and SPH simulation at $t=2.7\text{s}$

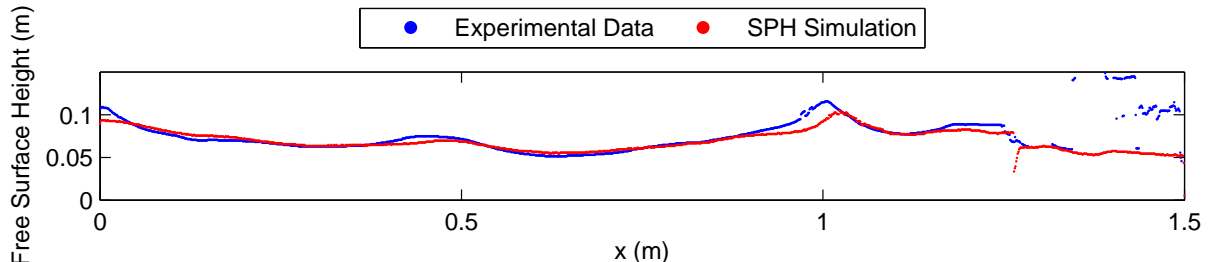


Figure A.33: Free Surface Profiles of Experimentation and SPH simulation at $t=6.5\text{s}$

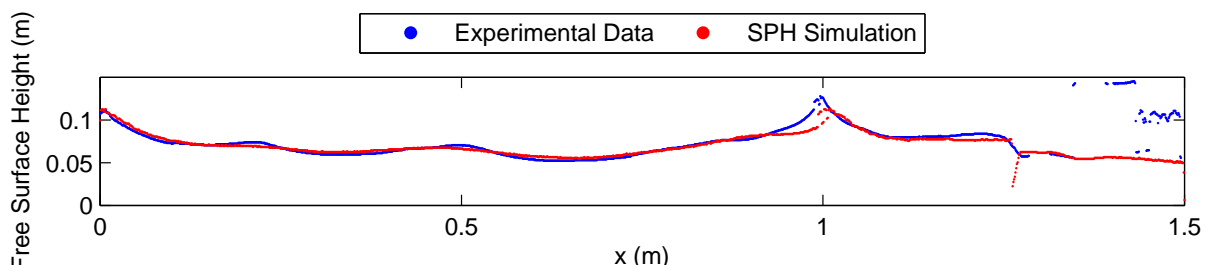


Figure A.34: Free Surface Profiles of Experimentation and SPH simulation at $t=11.5\text{s}$

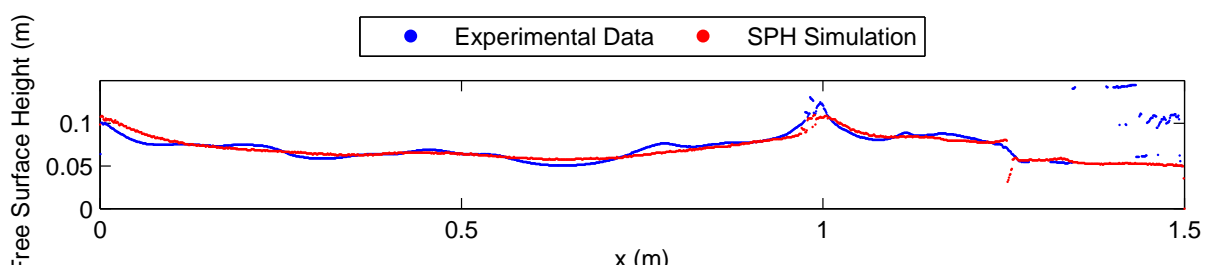


Figure A.35: Free Surface Profiles of Experimentation and SPH simulation at $t=17.8\text{s}$

B.2.2 1 in 2 Slope

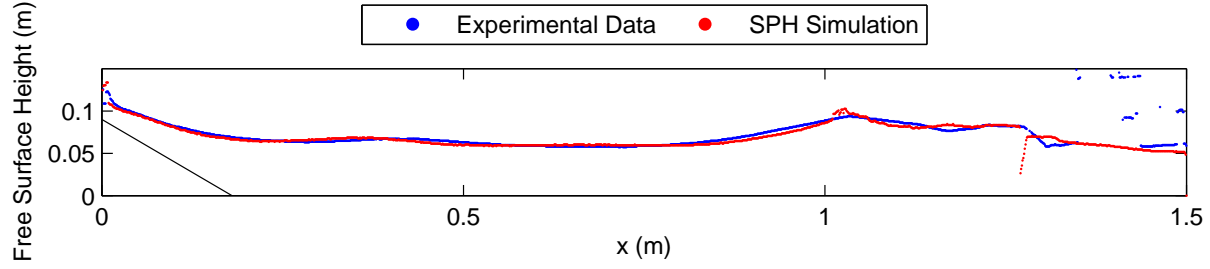


Figure A.36: Free Surface Profiles of Experimentation and SPH simulation at $t=2.7\text{s}$

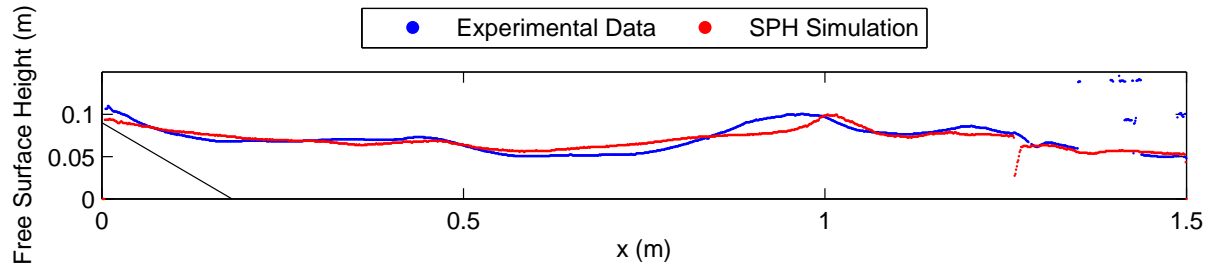


Figure A.37: Free Surface Profiles of Experimentation and SPH simulation at $t=6.5\text{s}$

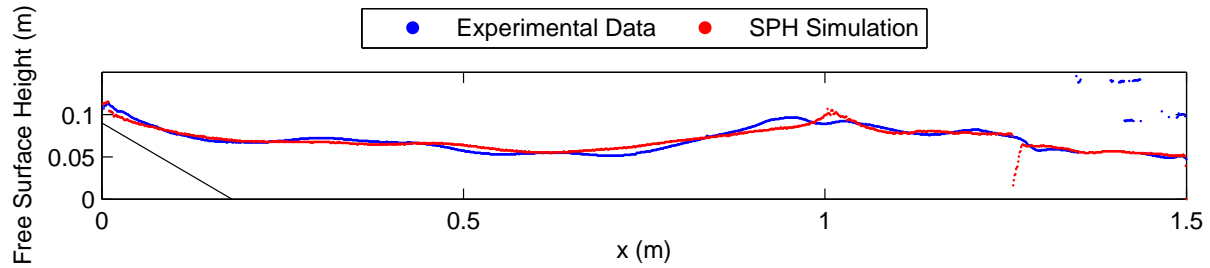


Figure A.38: Free Surface Profiles of Experimentation and SPH simulation at $t=11.5\text{s}$

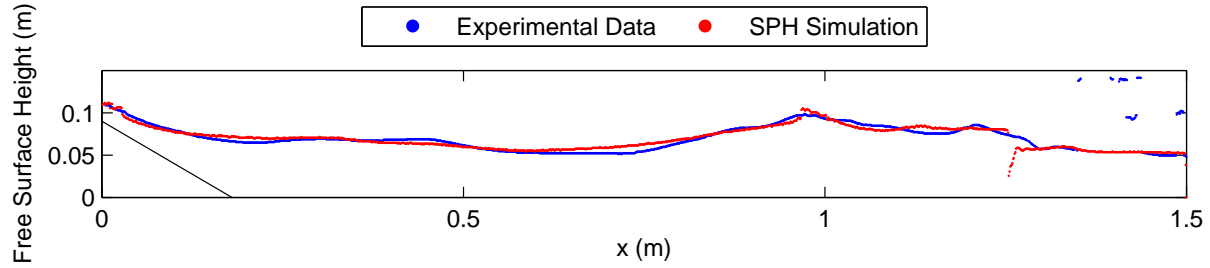


Figure A.39: Free Surface Profiles of Experimentation and SPH simulation at $t=17.8\text{s}$

B.2.3 1 in 3 Slope

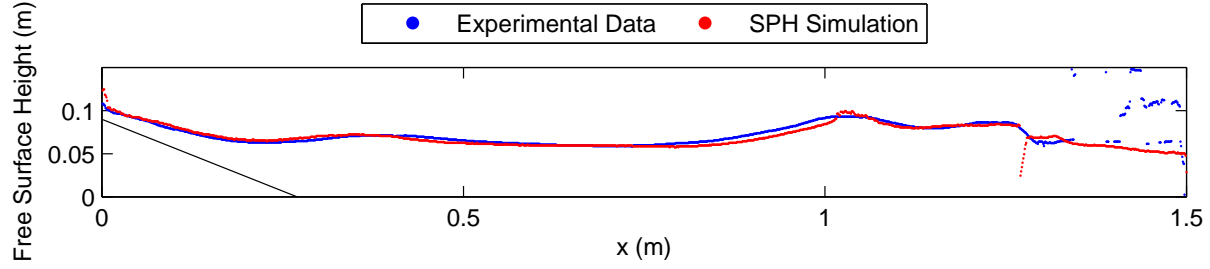


Figure A.40: Free Surface Profiles of Experimentation and SPH simulation at $t=2.7\text{s}$

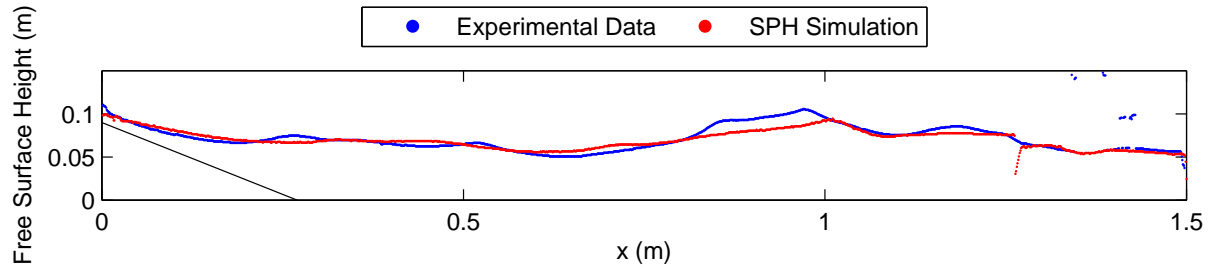


Figure A.41: Free Surface Profiles of Experimentation and SPH simulation at $t=6.5\text{s}$

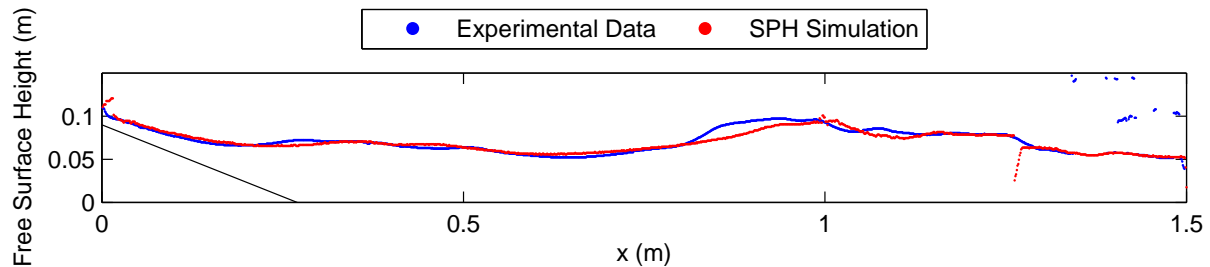


Figure A.42: Free Surface Profiles of Experimentation and SPH simulation at $t=11.5\text{s}$

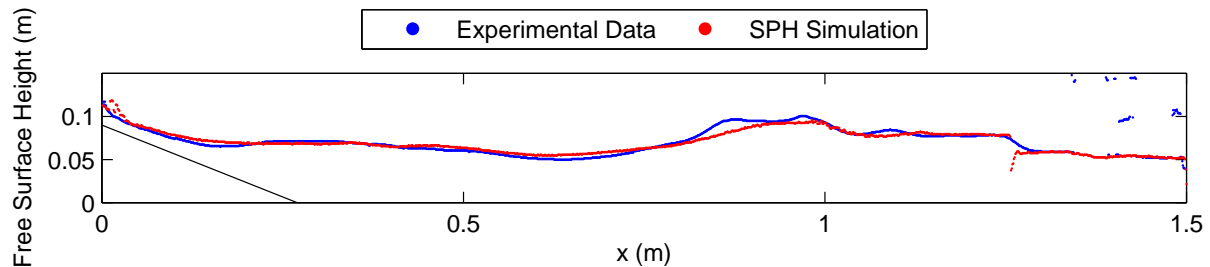


Figure A.43: Free Surface Profiles of Experimentation and SPH simulation at $t=17.8\text{s}$

B.2.4 Stepped Slope

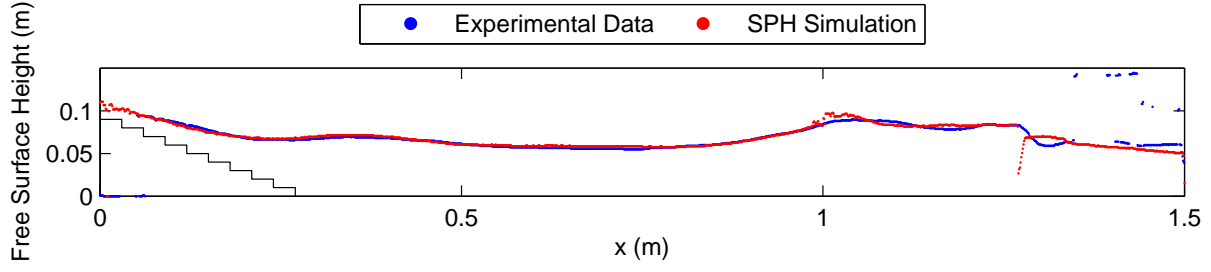


Figure A.44: Free Surface Profiles of Experimentation and SPH simulation at $t=2.7\text{s}$

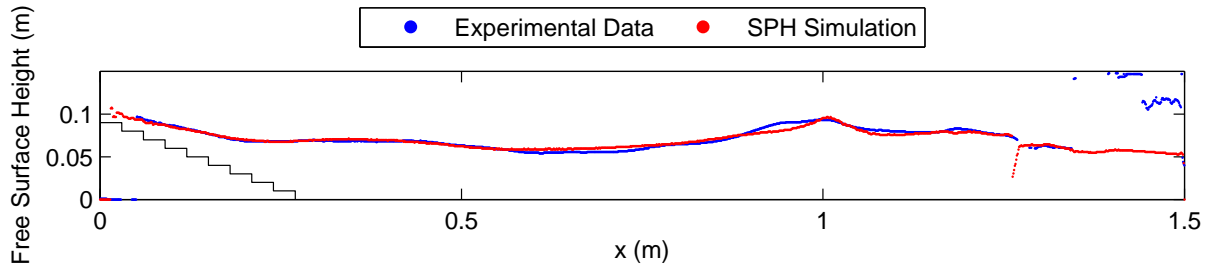


Figure A.45: Free Surface Profiles of Experimentation and SPH simulation at $t=6.5\text{s}$

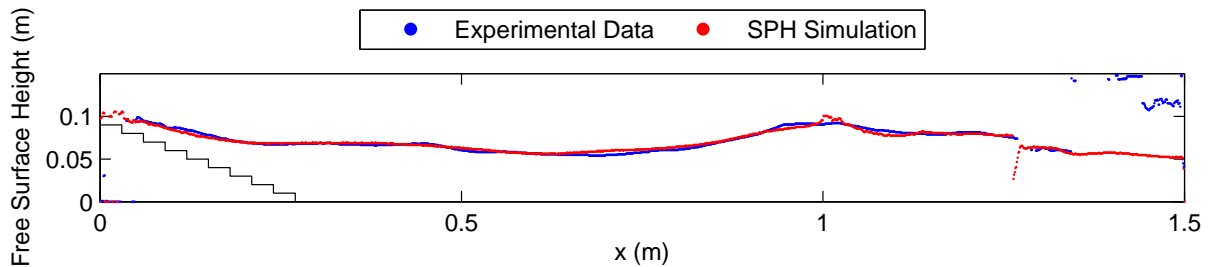


Figure A.46: Free Surface Profiles of Experimentation and SPH simulation at $t=11.5\text{s}$

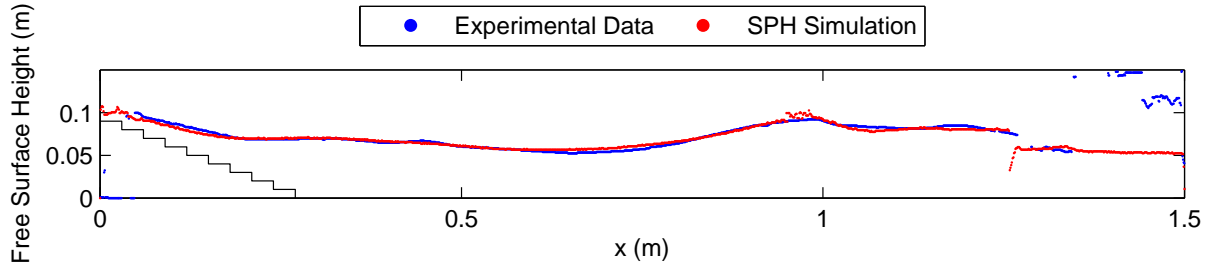


Figure A.47: Free Surface Profiles of Experimentation and SPH simulation at $t=17.8\text{s}$

B.2.5 Recurved Wall

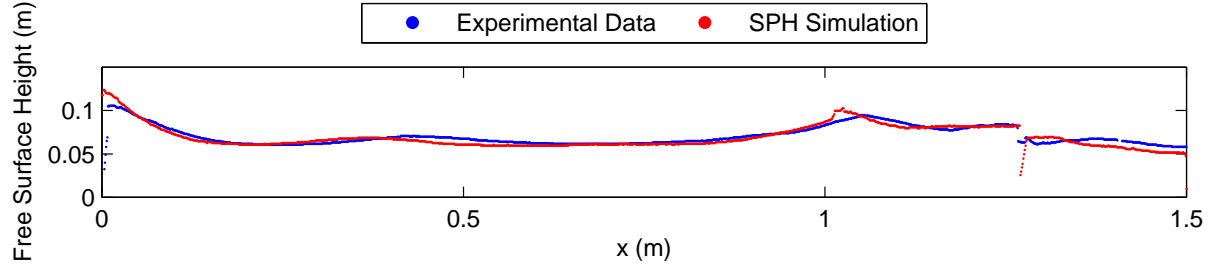


Figure A.48: Free Surface Profiles of Experimentation and SPH simulation at $t=2.7\text{s}$

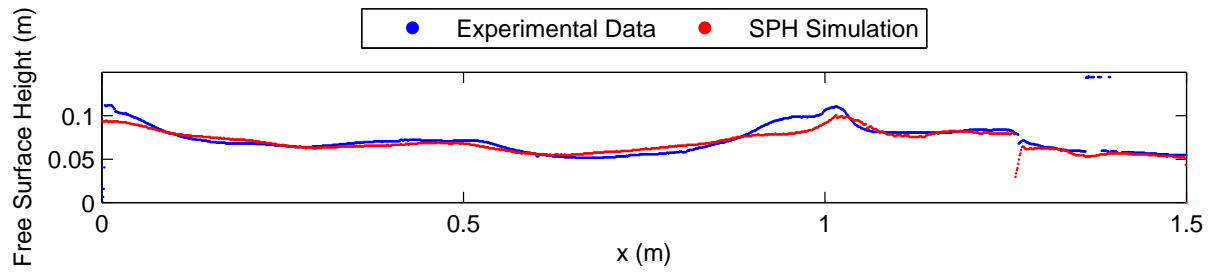


Figure A.49: Free Surface Profiles of Experimentation and SPH simulation at $t=6.5\text{s}$

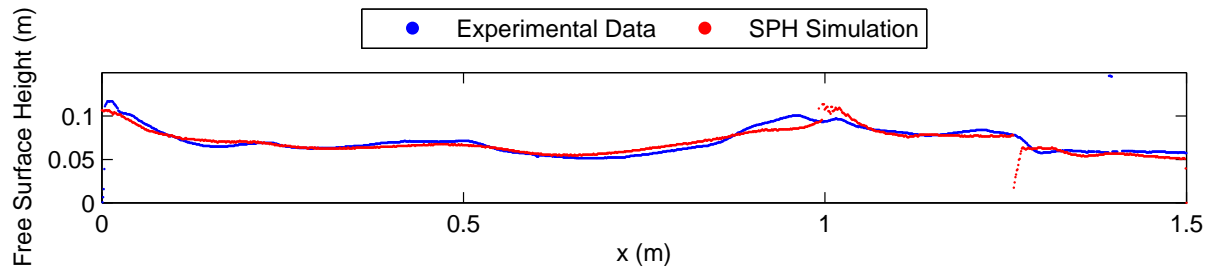


Figure A.50: Free Surface Profiles of Experimentation and SPH simulation at $t=11.5\text{s}$

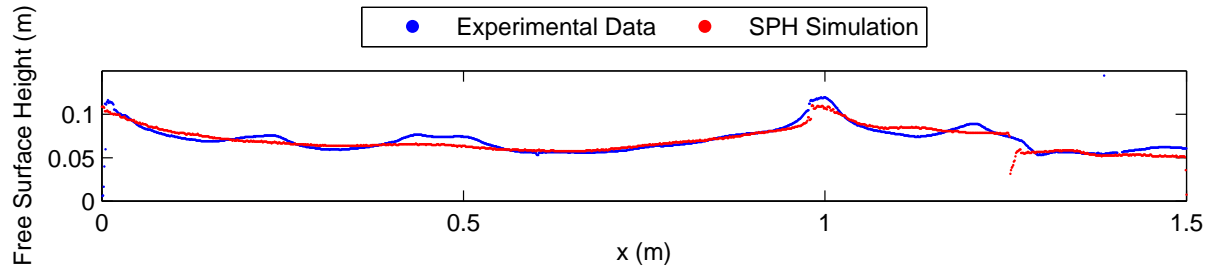


Figure A.51: Free Surface Profiles of Experimentation and SPH simulation at $t=17.8\text{s}$